

Navigating the Evolution of Two-dimensional Carbon Nitride Research: Integrating Machine Learning into Conventional Approaches

Deep Mondal^a, Sujoy Datta^{b,**}, Debnarayan Jana^{a,**}

^a*Department of Physics, University of Calcutta, 92 A. P. C. Road, Kolkata-700009, India*

^b*Kadihati KNM High School, P.O. Ganti, Kolkata-700132, India*

Abstract

Carbon nitride research has reached a promising point in today's research endeavours with diverse applications including photocatalysis, energy storage, and sensing due to their unique electronic and structural properties. Recent advances in machine learning (ML) have opened new avenues for exploring and optimizing the potential of these materials. This study presents a comprehensive review of the integration of ML techniques in carbon nitride research with an introduction to CN classifications and recent advancements. We discuss the methodologies employed, such as supervised learning, unsupervised learning, and reinforcement learning, in predicting material properties, optimizing synthesis conditions, and enhancing performance metrics. Key findings indicate that ML algorithms can significantly reduce experimental trial-and-error, accelerate discovery processes, and provide deeper insights into the structure-property relationships of carbon nitride. The synergistic effect of combining ML with traditional experimental approaches is highlighted, showcasing studies where ML driven models have successfully predicted novel carbon nitride compositions with enhanced functional properties. Future directions in this field are also proposed, emphasizing the need for high-quality datasets, advanced ML models, and interdisciplinary collaborations to fully realize the potential of carbon nitride materials in next-generation technologies.

Keywords: Carbon nitrides, Machine Learning models, Model training, Generative AI, Applications, Future prospects

1. Introduction

Since the debut of graphene [1], the landscape of material science has been forever altered, with the realm of two-dimensional (2D) materials emerging as an enduring focal point, captivating the research community for more than two decades now. Given its ubiquity and potential, nitrogen's prevalence alongside carbon renders CNs a prime candidate for cutting-edge research endeavors. Continuing its relevance to date, carbon nitrides owe much to their

*DM and SD contributed equally to this work

**Corresponding author

Email addresses: sujoydatta13@gmail.com (Sujoy Datta), djphy@caluniv.ac.in (Debnarayan Jana)

Abbreviation	Definition	Abbreviation	Definition
2D	Two-dimensional materials	MLIP	Machine Learning Interatomic Potential
CN	Carbon Nitrides	ELM	Extreme Machine Learning
PBE	Perdew-Burke-Ernzerhof	HSE	Heyd-Scuseria-Ernzerhof
DFT	Density Functional Theory	DOS	Density Of States
SCAN	Strongly Constrained and Appropriately Normed	ILs	Ionic Liquids
vdW	van der Waals	TEM	Transmission Electron Microscopy
XPS	X-ray Photoelectron Spectroscopy	STS	Scanning Tunneling Spectroscopy
PPL	Poly-Propio-Lactone	USPEX	Universal Structure Predictor
GNN	Graph Neural Network	KNR	k-Nearest Neighbors Regression
(K)RR	(Kernel) Ridge Regression	GBR	Gradient Boosting Regression
XGBoost	Extreme Gradient Boosting Regression	SVR	Support Vector Regression
LASSO	Least Absolute Shrinkage and Selection Operator	RF	Random Forest Strategy
SVM	Support Vector Machine	GPR	Gaussian Process Regression
ReLU	Rectified Linear Unit	PCA	Principal Component Analysis
AIMD	Ab-Initio Molecular Dynamics	NNP	Neural Network Potential
SAC	Single Atom Catalysts	TM	Transition Metals
SISSO	Sure Independence Screening	PSO	Particle Swarm Optimization
ECL	Electro-Chemie-Luminescence	TENG	Triboelectric Nanogenerators
DIMG	Deep Inorganic Material Generator	GT4SD	General Toolkit for Scientific Discovery

Table 1: **List of Abbreviations**

favorable experimental feasibility and diverse array of captivating attributes. From Dirac cone-like crossings to moderate semiconducting bandgaps, rich topological signatures to optical tunability across the whole visible spectrum, efficient thermal transport to surprisingly adept thermoelectric performances – their multifaceted nature promises continued exploration and innovation [2, 3, 4, 5, 6, 7]. For example, the widely studied graphitic carbon nitride (g- C_3N_4) and its favorable attributes including its tunable optoelectronic properties has been applied in a diverse range of fields like photocatalysis, sensing and photovoltaics [8, 9, 10]. The ongoing quest on this green energy material and its application has also been discussed in detail in different topical reviews [11, 12, 13, 14, 15]. Along with g- C_3N_4 , structural intricacies and respective stoichiometry of other 2D CN materials and their functionalized versions have been extensively studied. In 2016 and 2017, the successive experimental large-scale synthesis of crystalline, hole-free, semiconducting single-layer of C_3N or famously known as 2D polyaniline by two different groups adapting distinct synthesis [16, 17] routes has notably pushed the limits further. It is a graphene-like honeycomb lattice with a homogeneous distribution of C and N atoms with a D_{6h} symmetry. Despite the vast majority of C_xN_y materials, C_3N is the only one with a smaller indirect bandgap (0.39 eV) that exhibits ultrahigh stiffness (388 GPa-nm), low thermal conductivity ($128 \text{ W m}^{-1} \text{ s}^{-1}$), low-temperature ferromagnetism and optical tunability throughout the visible spectrum with excitonic dark and bright states [18]. This equivalent nitride of graphene finds its distinctive ingenuity in multiple aspects – from energy harvesting to nanoelectronics [19, 20]. Monolayers like C_2N [21, 22], C_4N [23], g- C_4N_3 [24, 25], C_6N_7 [26, 27] are already established to be versatile and adaptable to various sectors whether it is academia or industry.

Apart from the single layer C_xN_y networks, another very effective strategy to modulate and manipulate the material features has been the formation of heterojunctions or van-Der-Waals heterobilayers which facilitates easy exfoliation [28]. From an optoelectronic perspective, a very crucial factor is the presence of interlayer coupling which is necessary to mix different orbitals to justify the optical selection rules. For a g- C_3N_4 bilayer, it is reported that the primary bandgap gets increased by the interlayer coupling and the computed optical absorption depicts higher visible-light absorption [29]. In 2021, Wei *et al.* [30] critically explored, both via theoretical and experimental techniques, the bandgaps of bilayers of two-dimensional C_3N which can be engineered by controlling the stacking order or applying an electric field. Synthesis of AA' and AB' stacked C_3N are found to have different bandgaps with controllable on/off ratios, high carrier mobilities and photoelectric detection abilities. Apart from that, an in-plane conjugated heterostructure of C_2N/C_3N or vertically stacked type-II C_6N_6/C_3N_4 with a reduced band gap turned out to be an efficient HER (hydrogen evolution reaction) [31, 32]. A CN/C_3N_2 heterostructure has shown significant sensitivity towards SF_6 decomposed gases where one cell of this hetero-bilayer can capture eight of each gas with good adsorption strength [33]. Functionalizing the surface of the C_xN_y networks by heteroatom doping or just a stable ground state of CNs distinctly morphed with different stoichiometries has shown rich features to ponder. The effect of heteroatom doping for modulating the electronic structure has enormously enhanced the catalytic and electrochemical activities of different carbon nitride systems and their distinctive hybrids [34]. Along with others, Si doping has also been an efficient way to improve photocatalytic and electrocatalytic performance with suitable adsorption energies and activ-

ities [35, 36, 37]. Emergence of a special ‘dumbbell’ morphology is continuing to demand greater observation and recognition [6, 38, 39]. So this is really an ongoing quest.

Besides the conventional methods of study, the material science research is entering a brand new phase following the advent of artificial intelligence and machine learning (ML) [40]. ML essentially uses huge amount of datasets to iteratively optimize models and make reasonable predictions. The burgeoning application of ML in semiconductor discovery and catalysis research may pave the way for green energy revolution [41]. Although the advancement of application of ML methods on CNs is in its initial stage, its prospect is undoubted [42, 43]. Molecular dynamics simulations combined with ML algorithms are able to predict the free energy of exfoliation and solvation free energy for the liquid–phase exfoliation (LPE) of the g-C₃N₄ sheets [44]. It reduces the need to run additional lengthy computations. In fact, the identification of benzyl alcohol as a promising solvent was never incorporated previously for the LPE of 2D CNs. The bandgap of graphitic carbon nitride (GCN) subjected to external dopants under different experimental conditions are modeled using extreme machine learning (ELM) based models and hybrid support vector regression and genetic algorithm [45] where all models utilize a specific surface area as a descriptor for estimating bandgap energy. This integration of ML methodologies with CNs has emerged as a key strategy to advance their applications across diverse fields of materials science. In catalysis, ML models play a crucial role in the rational design of CN based photocatalysts for applications such as environmental remediation and hydrogen generation, leveraging predictive capabilities to enhance efficiency and selectivity. Furthermore, ML-driven simulations facilitate the exploration of CNs in energy storage systems, optimizing parameters such as conductivity and charge storage capacities. In materials discovery, ML algorithms aid in the systematic exploration and discovery of novel CN structures with tailored properties, thereby accelerating the innovation cycle in material science. This synergistic approach underscores the transformative potential of integrating ML with CNs, paving the way for advancements in sustainable technology and materials development.

In this topical review, we have aimed to critically discuss the arrival of 2D carbon nitrides, their ever-increasing popularity, high synthetic feasibility as well as the application perspectives alongside their future prospects focusing on the highly manifesting power of ML modelling. We will focus on how this technique can help to speed-up, predict and compute different aspects of this family of materials that can unquestionably push the boundaries further. Table-1 displays all the abbreviations and subsequent definitions that we have used throughout the article.

2. All about carbon nitrides

Now delving into the details of different CNs whether 2D monolayers or distinctly stacked bilayers, we will classify all existing C_xN_y materials as per their electronic nature. Tuning the C:N proportion, introducing structural defects, through heteroatom doping, different lattice symmetries or stacking monolayers consequently lead to rich electronic structure - from metals and wide bandgaps to half-metallicity or topologically protected semi-metals as shown in Figure-1.

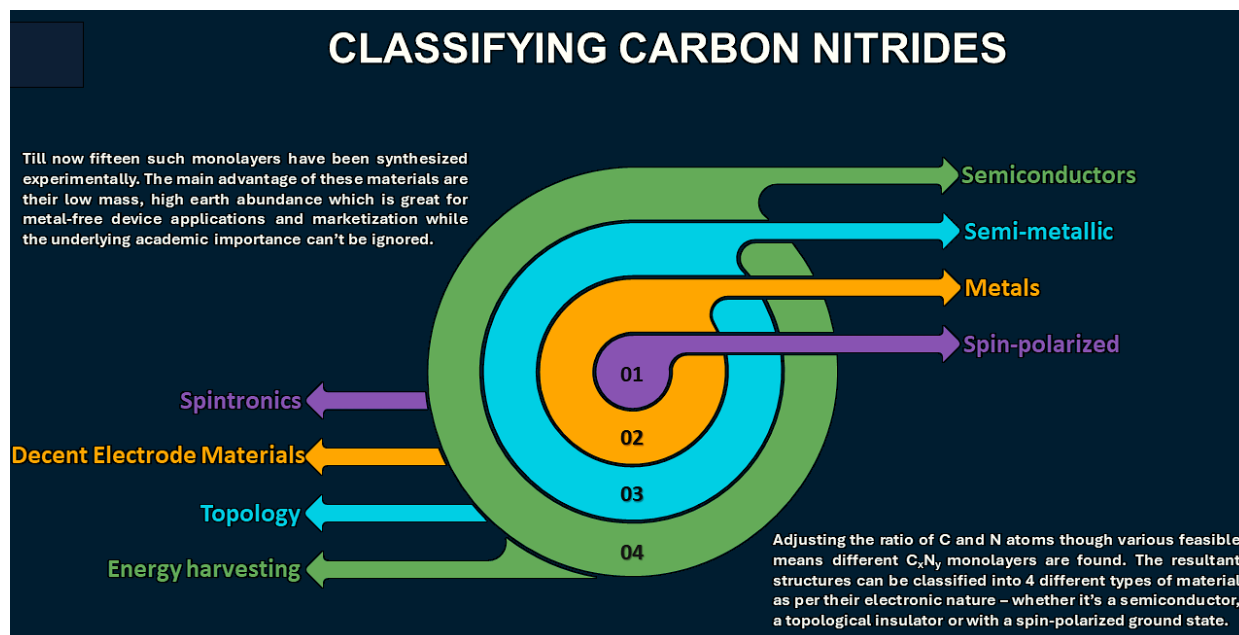


Figure 1: A schematic classification of existing monolayer carbon nitrides (both experimentally synthesized and theoretically proposed) based on their distinct electronic nature from semiconducting, metallic to semi-metallic and magnetic (or spin-polarized) ground states with plausible genres of application.

2.1. Semiconductors

A single layer of CN with a 1:1 proportion of C and N, namely graphitic nanoporous CN has been synthesized successively via the reactions of $C_3N_3Cl_3$ and Na by a simple solvothermal method [46] or by a simple polymerization of 3-amino-1,2,4-triazine [47]. As far as the lattice symmetry and parameters are concerned, single layer and non-magnetic g-CN possesses a hexagonal unit cell with equal a and b where $a=b=7.118 \text{ \AA}$ with an underlying symmetry group of P6/mmm. The g-CN monolayer has a direct band gap of 1.57 eV (PBE) and 3.18 eV (HSE06) [48] whereas the experimentally realized bandgap shows a value of 2.73 eV [46, 47]. It appears to have a very high surface-to-volume ratio and decent physiochemical stability [49, 50], as it has broad application prospects in the field of hydrogen storage [51] and electrocatalyst [52]. There is also a sp^3 hybridized three-sublayer crystal structure with four-coordinated carbon atoms, namely Tetra-Hexa CN_2 sandwiched between two sublayers of three-coordinated nitrogen atoms. The rectangular unit cell contains 12 atoms - four C and eight N atoms. The optimized lattice constants are $a = 4.18 \text{ \AA}$ and $b = 5.78 \text{ \AA}$. The buckling length between the two N layers is 1.48 \AA . This material is isostructural to the tetra-hexa-carbon [53] but with reduced lattice constants and increased buckling. Electronically, TH- CN_2 is a wide indirect gap semiconductor with a value of 4.57 eV as per the more accurate HSE06 functional [54]. A similar stoichiometric monolayer, Penta CN_2 which is a nitrogen-rich (nearly 21.66%) material with a tetragonal lattice with a lattice constant $a = 3.31 \text{ \AA}$ and belongs to a crystal group of P-42₁m layer group number-58 [55]. The relaxed structure of penta- CN_2 is composed of three layers of C atoms in the middle and N atoms on the top and

bottom [56] - analogous to well-known B_2C (1.08 Å) [57] or SiC_2 (1.33 Å) [58] etc. This single layer also possesses a large indirect bandgap semiconductor with a bandgap value of 4.83 eV (PBE) and 6.53 eV (HSE06). Penta-CN₂ also displays an interesting double degeneracy along the first Brillouin zone edges, which is topologically protected by the nonsymmorphic symmetry of the structure.

The hexagonal unit cell of C_2N is constructed in chain-like rings and the hexagonal rings are linked via the C-N bond. The optimized lattice constant of the C_2N monolayer is estimated to be of 8.33 Å. In 2015, Mahmood *et al.* reported the preparation of layered two-dimensional C_2N via a simple wet-chemical reaction [59]. It was prepared by mixing hexa-amino-benzene (HAB) trihydrochloride and hexa-keto-cyclohexane (HKH) octahydrate in N-methyl-2-pyrrolidone. The consequent material was dark black and exhibited experimental direct bandgaps of 1.96 eV which closely agrees with the theoretical calculations (1.7 eV). Figure-2 below displays all the necessary experimental findings.

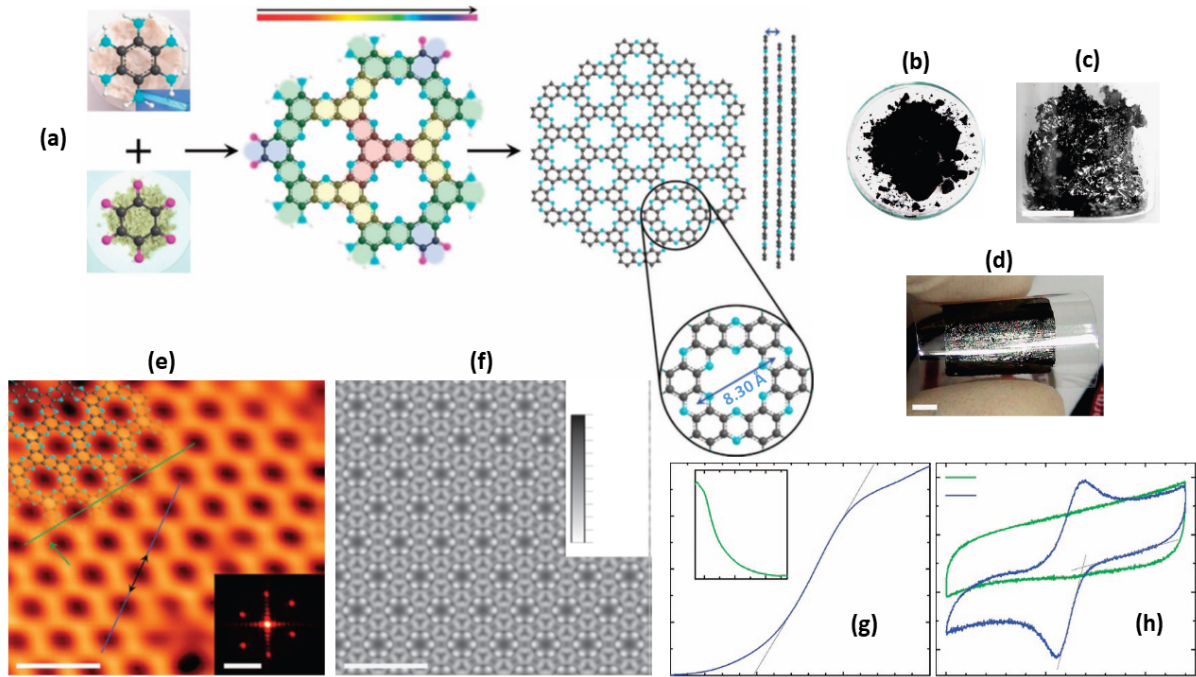


Figure 2: (a) Schematic representation of the reaction between hexaaminobenzene (HAB) trihydrochloride and hexaketocyclohexane (HKH) octahydrate to produce the C_2N -h2D crystal. The inset in the image of HAB is a polarized optical microscopy image of the HAB single crystal. Digital photographs: (b) as-prepared C_2N -h2D crystal; (c) solution-cast C_2N -h2D crystal on a SiO_2 surface after heat-treatment at 700°C; (d) a C_2N -h2D crystal film (thickness: approximately 330 nm) transferred onto a PET substrate. The shiny metallic reflection of the sample indicates that it is highly crystalline. Figure-(e,f) shows the atomic-resolution STM topography image of the C_2N -h2D crystal on Cu(111). The STM image was obtained at a sample bias of 0.7 V and a tunnelling current of 300 pA. The top-left inset is the structure of the C_2N -h2D crystal superimposed on the image. The bottom-right inset is 2D fast Fourier transform and the simulated image respectively. Figure-(g,h) show the results of optical band-gap measurements and a plot of the absorbance squared vs. photon energy extrapolated to zero absorption. The inset is the ultraviolet absorption curve. (b) Cyclic voltammograms of the C_2N -h2D crystal at a scan rate of 100mVs⁻¹ using a Ag/Ag⁺ reference electrode. Reprinted with permission from [59] Copyright 2015, Nature

Ever since its successful synthesis, reports on using C_2N materials have flourished quite drastically [60]. Lei Wang *et al.* reported a metal-free Z-scheme preparation for water splitting using C_2N and aza-fused microporous polymeric nanosheets in 2018 [61], highlighting the potential of the polymer photocatalyst. This Z-scheme plays a vital role in photocatalytic reactions that require both reducing and oxidizing capabilities. For instance, in photocatalytic water splitting, light energy drives the separation of water into hydrogen and oxygen. The Z-scheme facilitates efficient separation and transfer of photogenerated charge carriers between two different semiconductors, enabling the simultaneous reduction of protons to hydrogen and oxidation of water to oxygen. This mechanism is crucial for designing efficient photocatalytic systems for applications such as solar fuel production and environmental remediation. Especially, C_2N has been reported to be quite superior in terms of elasticity compared to the other two allotropes, namely heptazine and s-triazine [62]. A recent report has displayed its tetragonal counterpart namely $T-C_2N$ which has a relaxed lattice parameter of 5.99 Å and electronically possesses a smaller indirect bandgap of about 0.73 eV [63]. The unstable puckered N nanosheet (i.e. bp-N monolayer) has been stabilized by inserting C_2 dimers between the upper and lower N zigzag lines which in turn forms C_2N_2 nanosheet possesses good energetic, dynamical and thermal stability [64]. The relaxed unit cell of C_2N_2 sheet is orthogonal having lattice parameters of 3.46 and 2.39 Å in two different directions with a space group of Pmna (53). This is an anisotropic indirect gap semiconductor of value 2.56 eV (SCAN) and 3.58 eV (HSE06) with simultaneous traces of ultrahigh carrier mobilities and large in-plane anisotropy. A large anisotropic mobility ratio of 85 for the hole mobility of bp- C_2N_2 nanosheet is discovered - the maximum anisotropy value reported for a 2D material.

A C_2N_3 unit cell has an optimized lattice parameter of 7.864 Å which has a total 12 C atoms and 18 N atoms with the underlying P6/mcm space group [65]. It shows a heavily doped p-type semiconductor characteristic with an indirect bandgap of 4.62 eV (in HSE06) and 3.26 eV as per PBE functional. In 2017, Miller *et al.* synthesized single-layer of CN nanosheets with an approximately close stoichiometry of C_2N_3 via the spontaneous dissolution of bulk PTI based carbon nitride [66].

For the family C_3N_x ($x = 1-7$), Baek and co-workers reported the synthesis of 2D C_3N from the direct pyrolysis of hexa-amino-benzene trihydrochloride (HAB) single crystals at 500°C for 2 hr [16] as shown in Figure-3 with topographical images and underlying electronic spectra. They studied the C_3N formation mechanism in detail, which involved the evolution of ammonia and ammonium chloride. Yang *et al.* reported a controllable large-scale synthesis of C_3N quantum dots by 2,3-diaminophenazine polymerization through hydrothermal process [17]. The polymerization steps were identified by Matrix-Assisted Laser Desorption Ionization - Time of Flight Mass Spectroscopy (MALDI-TOFMS). The well-crystallized unit cell of graphene-like C_3N possesses a honeycomb structure with a lattice constant of 4.86 Å and the two-fold hexagonal single crystal form indicates D_{6h} -symmetry of the N and C atoms. It is a small bandgap indirect semiconductor (1.23 eV in HSE06 and 0.39 eV in PBE) with ultrahigh stiffness (higher than graphene) and traces of low-temperature ferromagnetism (below 96 K) with hydrogen doping.

Its tetragonal counterpart possesses a wide and direct semiconducting gap of 5.74 eV with a proper pore size of 5.5 Å - perfect for water infiltration [67]. In a recent work of ours, we have critically analyzed and reported

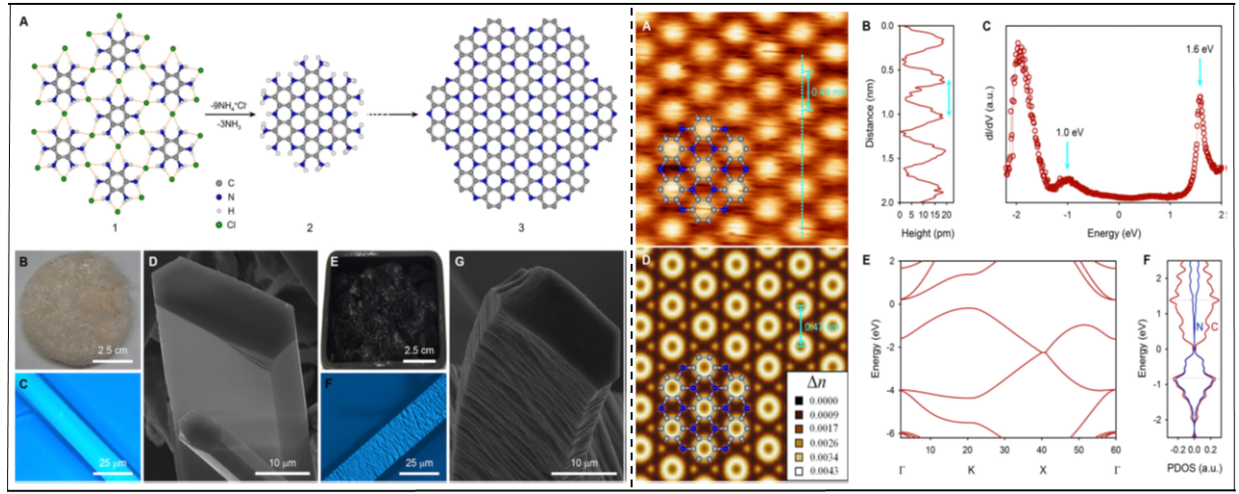


Figure 3: In the left panel the schematic representation of 2D PANI formation is shown here. (A) Single-crystal X-ray packing structure of HAB (structure-1); structure of 2D PANI unit with edge groups (C_3NH , structure-2), and the spontaneous transformation of HAB crystal unit into the 2D PANI structure (structure-3). Morphology changes of HAB crystals into 2D PANI frameworks. (B) Digital photograph of HAB crystals on butter paper. (C) Optical microscopy image of a needle-like HAB crystal before annealing. (D) SEM image of an HAB single crystal before annealing. (E) Digital image of HAB after annealing at 500°C . (F) Optical microscopy image of 2D PANI crystal after annealing at 500°C . (G) SEM image of a 2D PANI single crystal after annealing. STM and theoretical studies of the 2D PANI structure. In the right panel - (A) STM image of a 2D PANI framework ($2.5 \times 2.5 \text{ nm}^2$, $V_s = -1.1 \text{ V}$, $I_t = 1.0 \text{ nA}$). Inset structure represents C_3N repeating unit with carbon atom (gray ball) and nitrogen atom (blue ball). (B) Topographic height profile along the cyan dot line marked in A. (C) Differential conductance (dI/dV) spectrum of a 2D PANI framework. (D) Simulated STM image with superimposed structure of C_3N repeating unit. (E) Electronic band structure. (F) PDOS of the carbon (dark red) and nitrogen (dark blue) atoms. Reprinted with permission from [16] Copyright 2016 PNAS.

spontaneous dumbbell formations from monolayer C_3N which contains three indirect gap semiconductors (about 2-3 eV) of dumbbell C_3NX ($X = B, P$ and As) [6].

Porous graphitic C_xN_y monolayers with semiconducting features have drawn wider attention over the years because of built-in pores with active sites and larger surface area. Only a few such CNs have been synthesized - covering the bandgap range of 1.23–3.18 eV. A recent study systematically investigates two new 2D monolayers Tetra- and hexa- C_3N_2 with realistic pathways for their experimental realization [68]. The relaxed structures of H- and T- C_3N_2 comprise lattice parameters of 12.29 Å and 8.63 Å with subsequent space groups P6/mmm and P2/m respectively. The underlying electronic depicts the direct bandgap nature of about 0.35 eV (T- C_3N_2) and 1.97 eV (H- C_3N_2) as per HSE06 functional which are nearly double that of in PBE with high carrier mobilities and excellent visible-light absorption.

For the graphitic C_3N_3 cell, every six C_3N_3 rings enclose a pore in C_3N_3 layer. The C-C and C-N bond lengths are 1.51 Å and 1.34 Å respectively with the optimized lattice parameters of 7.11 Å. The diameter of the pore is 5.46 Å, almost the same as that of the one in graphdiyne (5.42 Å). The pore edge is surrounded by 6 N atoms with zero dangling bonds. The band structure shows a direct band gap of 1.60 eV. This assembled CN network has also been realized experimentally through a simple solvothermal technique with well-controlled dimensionality

and luminescence [46]. Carbon nitride nanotube bundles were formed using NiCl_2 as a catalyst precursor while the reaction of cyanuric chloride ($\text{C}_3\text{N}_3\text{Cl}_3$) with sodium at 230°C and 1.8 MPa is taking place in a stainless steel autoclave.

Graphitic carbonic nitride ($\text{g-C}_3\text{N}_4$) has attracted much attention since it was first constructed to be a visible-light-driven photocatalyst due to its high abundance, stability and decent capacity for solar utilization [69]. In the realm of energy conversion and storage, the unique layered structure of $\text{g-C}_3\text{N}_4$, along with its tunable bandgap, metal-free nature, high physicochemical stability, and ease of synthesis, have significantly contributed to its growing popularity including batteries and supercapacitors. [70, 71, 49]. The porous structure plays a crucial role in enhancing the performance of negative electrodes in lithium-ion batteries. Pan *et al.* explored $\text{g-C}_3\text{N}_4$ nanotubes with porous architectures through a first-principles study. These porous structures shorten the diffusion pathways for Li^+ ions during lithiation and delithiation processes, enabling the material to achieve a relatively high specific capacity of up to 1165.3 mAh/g [72]. However, its high nitrogen content has led to challenges such as poor conductivity and substantial irreversible capacity loss. To address these issues, Chen *et al.* introduced a magnesiothermic denitrating technique to reduce the nitrogen content of $\text{g-C}_3\text{N}_4$, enhancing its performance as a lithium-ion battery anode [73]. This approach achieved a highly reversible lithium storage capacity of 2753 mAh/g after 300 cycles, with improved cycling stability and rate capability. Several phases of C_3N_4 (α, β, γ or cubic) with their structural formation, semiconducting electronic nature and photocatalytic activities have been reported and studied earlier [4]. A facile one-pot synthesis of nanoporous graphitic carbon nitride has been done using different soft and direct templates through the self-polymerization reaction of dicyandiamide (DCDA) [74]. This material was also realized experimentally by condensing melamine in air for 2 hr and the exfoliation is observed beyond 600°C . It was used for the photocatalytic decomposition of N_2O [75]. Figure-4 depicts the scanning and tunnelling electron microscope (SEM and TEM) images for $\text{g-C}_3\text{N}_4$ samples obtained at 600°C and 700°C . In 2022, $\text{g-C}_3\text{N}_4$ monolayer in the perfect 2D limit was successfully realized, for the first time, by the well-defined chemical strategy based on the bottom-up process [76]. In Figure-5 we can see all the details which includes schematic diagram of the synthesis using 2D Mica plate, XRD patterns, HRTEM, AFM imaging with the subsequent histogram for the size distribution of $\text{g-C}_3\text{N}_4$ -m.

Inspired by the polymerization of urea, the preparation of the novel C-C bridged heptazine CNs UO_x (x is the ratio of urea to oxamide, $x = 1, 1.5, 2, 2.5$ and 3) has been achieved, which is close to $(\text{C}_6\text{N}_7)_n$ for the first time by introducing part of oxamide. A simple and efficient process for the synthesis of 2D CNs and related materials of very high quality is reported which relies on the use of a metallic surface as both a reagent and a support for the coupling of small halogenated building blocks [77].

Now before delving into further results and their subsequent implications, the connection between porosity density and the ratio of nitrogen atoms in carbon nitride (CN) lattices needs to be addressed as it is quite crucial for understanding and optimizing the properties of these materials. The porosity density directly influences the available surface area and the pathways for ion diffusion, which are important for applications in energy storage [78], catalysis [79], and sensing [80]. A higher porosity typically enhances the material's capacity to adsorb and interact with molecules,

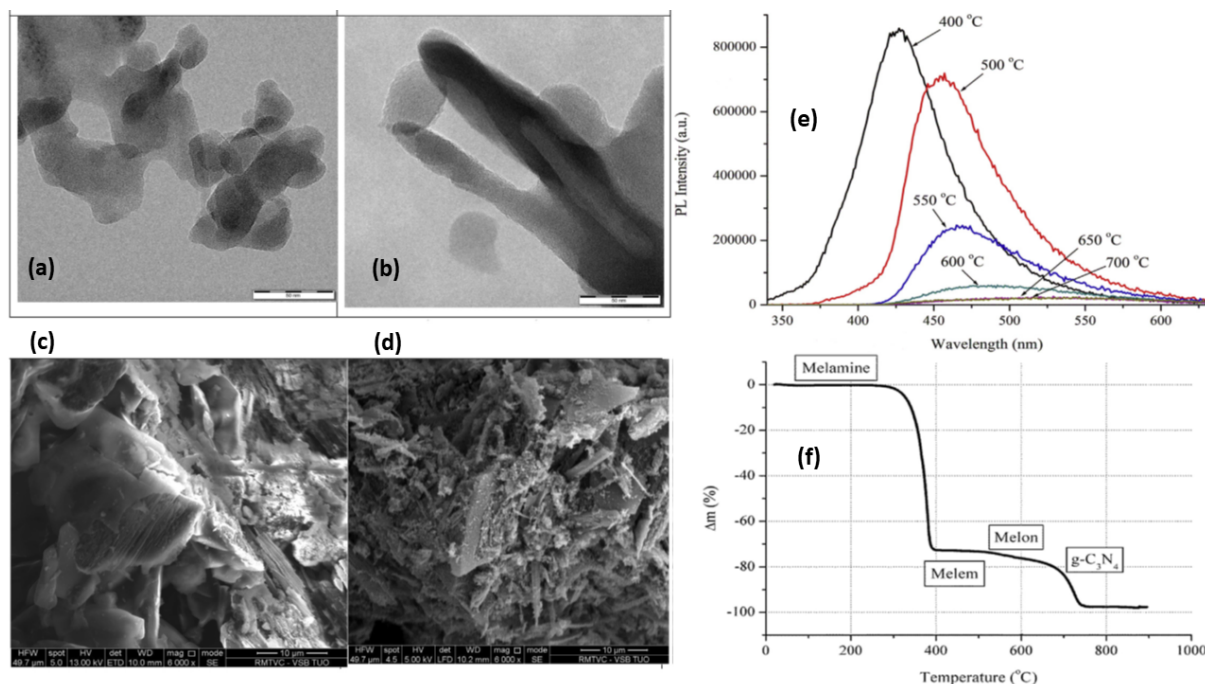


Figure 4: Figure-(a,b) and (c,d) shows the TEM and SEM images of g-C₃N₄ samples obtained at 600°C and 700°C. The photoluminescence spectra of melamine products obtained at different temperatures and the thermogravimetric curve of annealing of melamine are shown in figure-(e) and (f) respectively. Reprinted with permission from [75] Copyright 2017 Elsevier

improving its performance in catalysis and sensor applications. The ratio of nitrogen atoms in CN lattices also plays a significant role in modulating electronic properties [81]. Nitrogen doping in carbon materials can create localized states in the electronic structure, which can affect conductivity, charge storage capabilities, and catalytic activity. By adjusting the nitrogen content, it may be possible to tune the electronic structure, making CN materials more suitable for specific applications. For instance, higher nitrogen content can enhance the electrochemical performance of materials used in energy storage, as nitrogen can help stabilize lithium or sodium ions in batteries [82, 83]. Even from a mechanical standpoint, the porosity and nitrogen content can affect the material's stability, strength, and elasticity. In porous CN materials, the mechanical properties are often influenced by the distribution and connectivity of nitrogen atoms within the lattice, as well as by the pore size and structure. Nitrogen-rich graphitic carbon nitrides (g-C₃N₅) have emerged as promising star for photocatalytic applications due to its significant enhancements in light absorption properties, which can activate in ultraviolet, visible, and even under near-infrared irradiation [84]. This can also enhance the material's resistance to thermal degradation, making it more stable under high-temperature conditions, which is beneficial for catalysis, hydrogen evolution and energy storage applications [85, 86, 87]. In 2021, Liu *et al.* reported a series of 2D co-catalyst nitrogen-doped graphenes with the different bond states of doped nitrogen were synthesized under modified synthetic conditions, resulting in different surface catalytic hydrogen peroxide generation activities [88]. Table-2 properly showcases all the structural details, underlying symmetry, subsequent electronic

nature and synthesis (if yet synthesized or not) route taken with proper referencing.

2.2. *Semi-metallics:*

The emergence of Dirac points in 2D materials, or more specifically, in 2D CNs which are typically insulating, is rare. Moreover, the appearance of symmetry-protected nodal-line semimetal with sheer robustness against external strain is quite surprising. For example, in 2020, Tan *et al.* discovered a family of holey nitride monolayers namely C_xN_3 ($x=7,10,13,19$) with Dirac-like crossing exactly at the Fermi level. It has been constructed from a $\sqrt{13} \times \sqrt{13}$ graphene by removing a six-membered ring of carbon atoms - replacing the carbon atoms at the edge of the hole with nitrogen atoms. These four novel nanosheets belong to two distinct groups, namely space group P6mm (183) for $C_{10}N_3$ and $C_{13}N_3$ and P6 (168) for the other two structures. Another interesting occurrence is the traces of intriguing topological signatures in low-mass structural forms due to their weaker spin-orbit interaction. In recent years, a pool of such materials has been discovered with rich electronic structures carrying symmetry-protected semi-metallicity or quasi-1D Dirac nodal lines and topological flat edge states such as zigzag buckled C_4N [23], dumbbell C_3NX ($X = C, Si, Ge$) [89], C_xN_4 ($x = 4,5,9$) [90, 91, 92], $C_{19}N_3$ [93] etc. It has been suggested that experimentally the 1,3,5,7-Tetrazocine monomer and the dehydrogenation reaction of C_2H_4 and $C_4H_4N_4$ can be used to synthesize semimetallic C_4N_4 and C_5N_4 respectively. A very recent article reported a strong anisotropic Dirac state in monolayer TPH- C_5N_3 with non-zero \mathbb{Z}_2 invariant and topologically non-trivial edge states [94]. A possible synthetic pathway has also been proposed through dehydrogenation and polymerization while cyclobutadiene, pyrazine and tetra-aminoethylene are chosen as precursors. Table-2 has all the necessary details and subsequent references.

2.3. *Metals:*

One of the most recent members of the carbon-nitride family, monolayer C_5N , reported to be chemically, mechanically and thermodynamically stable is found to be metallic and reported to be a promising building block for the anode of Potassium-ion batteries [95]. In 2011, 2D C_5N_2 was synthesized successfully by Kou *et al.* [96] with a large surface area and high conductivity. Synthesis of such porous frameworks based on aza-fused CMPs were ionothermally realized by condensation of 1,2,4,5-benzenetetramine with triquinoyl hydrate from 300 to 500°C. In this year, allotropes of three novel C_5N_2 (type-a, b and c) are shown to have great potential as high-performance alkali metal ion battery material [97]. Recently, a planar and hybridized metallic structure with h57 Haeckelite orientation C_7N is proposed with consequent application in high-capacity anode for post-Li-ion batteries [98]. Apart from that, for C_9N_4 and $C_{10}N_3$, the Fermi level is found to be crossed by the σ ($s+p_x+p_y$) and π (p_z) orbitals of N and C atoms, leading to the formation of metallic character [99].

2.4. *Spin-polarized:*

Half-metals - displaying the feature of a metal in one spin channel and of a semiconductor in the other, have attracted some serious research attention due to their potential applications in the spintronic field over the years

[100, 101]. As far as the low-dimensional CNs are concerned, very few have been reported over the course of time. In the year 2010, a graphitic carbon nitride, namely, g-C₄N₃ was experimentally realized by Lee *et al.* [102] which interestingly can exhibit half-metallicity without any external modification and preserves the formational and magnetic stability even at 500 K [103]. Functional porous carbons were prepared via direct, ambient-pressure, thermal pyrolysis of task-specific ionic liquids (ILs). This process lies in the synergistic usage of the insignificant volatility of the ILs and the inclusion of the cross linkable nitrile groups in the anions. The resulting product retained an extremely high N content of about 18% at a temperature of 800⁰C. Incorporating hydrogen dangling bonds has also been reported to be a decent strategy to tune the magnetic features of metal-free g-C₃N₄ nanosheets [104]. A unique form of monolayer viz. dumbbell-C₇N₃ can be formed after substituting three N atoms in the dumbbell-C structure which showcases magnetism and the magnetic moment bears a value of 1 μ B. This is a specifically Bipolar magnetic semiconductor (BMS), where the valence and conduction bands possess opposite spin polarization with different bandgap values (direct gap of 0.9 eV for up-spin and indirect of 1.7 eV for spin-down). This type of material can control the gate voltage properly. Gao *et al.* in 2020 showed the emergence of ferromagnetism in graphitic carbon nitrides through nitrogen defects [105]. Table-1 here shows all different existing magnetic graphitic C_xN_y with necessary structural details with corresponding electronic nature whether a half-metal (HM), BMS or spin-polarized metal (SPM).

2.5. *Stacked bilayers and heterostructures:*

Layered stacking or lateral interfacing of atomic monolayers has opened up unprecedented opportunities to engineer 2D heteromaterials. Creating composites of two or more semiconductors (SCs) can often enhance charge separation, thereby improving catalytic efficiency. In typical composite materials, commonly referred as heterostructures, the two types of charge carriers are distributed across different components. This separation slows down electron-hole recombination and introduces a unique donor-acceptor band offset. Depending on the characteristics of this band offset and the direction of electron and/or hole transfer, these composite materials are categorized into three sub-types. For carbon nitrides, the last few years have been quite intriguing as far as the fabricated heterostructures are concerned and the rich outcomes have shown their promise. For example, the hydrogen evolution reaction (HER) via the electrocatalytic reduction of water has become a promising method for a green energy supply in the future. However, the carbon-based metal-free electrocatalysts show poor activity. In 2018, Xu and co-workers reported an in-plane heterostructure of two synthesized monolayers of C₂N and C₃N which showcases a directional transfer of electrons from C₃N to C₂N under the built-in potential and projects its potency as a metal-free photocatalyst [31]. Furthermore, g-C₃N₄-based type-II heterojunction photocatalysts have shown remarkable improvements in photocatalytic activity due to the effective spatial separation of electron-hole pairs enabled by the band alignment between two semiconductors. Their catalytic performance has been significantly boosted by employing the Z-scheme mechanism [134]. This Z-scheme plays a vital role in photocatalytic reactions that require both reducing and oxidizing capabilities. For instance, in photocatalytic water splitting, light energy drives the separation of water into hydrogen and oxygen. The Z-scheme facilitates efficient separation and transfer of photogenerated charge carriers between two dif-

Structure	a_0 (in Å)	Symmetry	Buckling (in Å)	Electronic nature (Type)	Bandgap (in eV - Theory/Expt.)	Synthesis (Method)	Reference
CN	7.12	Hexagonal	-	SC (Direct)	3.18/2.73	Y (Solvothermal or Polymerization)	[46, 106, 47]
Tetra-Hexa CN ₂	4.18 (and 5.78)	Rectangular	1.48	SC (Indirect)	4.57/-	-	[54]
Penta-CN ₂	3.312	Tetragonal	1.52	SC(Indirect)	6.53/-	-	[55, 107]
C ₂ N	8.33	Hexagonal	-	SC(Direct)	1.7/1.96	Y(Wet-chemical reaction)	[59, 60]
T-C ₂ N	5.99	Tetragonal	-	SC(Indirect)	0.73/-	-	[63]
C ₂ N ₂	3.46 (and 2.39)	Orthogonal	3.10	SC(Indirect)	3.58/-	-	[64]
C ₂ N ₃	7.864	Hexagonal	-	SC(Indirect)	4.62/-	Y (Spontaneous dissolution)	[65, 66]
C ₃ N	4.86	Hexagonal	-	SC(Indirect)	1.23/0.39	Y(Direct pyrolysis)	[30, 16, 17]
T-C ₃ N	3.38	Tetragonal	-	SC(Direct)	5.74/-	-	[67]
Dumbbell C ₃ NX	4.76-4.88	Hexagonal	1.92-3.62	SC (Indirect) and SM	2-3	-	[6]
H-C ₃ N ₂	12.29	Hexagonal	-	SC (Indirect)	1.97/-	-	[68]
T-C ₃ N ₂	8.63	Hexagonal	-	SC (Direct)	0.35/-	-	[68]
g-C ₃ N ₃	7.11	Hexagonal	-	SC (Direct)	1.6/2.2	Y (Solvothermal)	[108, 46, 109]
g-C ₃ N ₄	4.79	Hexagonal	-	SC (Indirect)	2.76/2.7	Y (Condensation/ Template)	[75, 74, 4]
g-C ₃ N ₅	15.203	Hexagonal	-	SC (Direct)	2.19/1.76	Y(Thermal deammoniation)	[110, 111, 112]
s-C ₃ N ₆	10.57	Hexagonal	-	SC(Direct)	2.59/-	Y (Low temperature pyrolysis-Nanotemplating)	[113, 114]
C ₃ N	7.69 (and 6.37)	Triclinic	-	SC (Direct)	0.82/-	Y (Low temperature pyrolysis-Nanotemplating)	[114]
C ₄ N	12.64	Hexagonal	-	SC (Direct)	1.80/2.55	Y (Hydrothermal solvent)	[115]
C ₄ N-I	5.44	Rectangular	-	SC (Direct)	0.09/-	-	[116]
C ₄ N-II	4.45	Rectangular	-	SM	-/-	-	[116]
ZB C ₄ N-I	4.747 (and 4.114)	Rectangular	1.55	DNL	-/-	-	[23]
ZB C ₄ N-II	4.741 (and 4.114)	Rectangular	1.54	DNL	-/-	-	[23]
g-C ₄ N ₃	4.81	Hexagonal	-	HM(Direct)	2.0/2.0	Y (Thermal pyrolysis)	[102, 103]
C ₄ N ₄	3.58 (and 6.10)	Rectangular	0.41	SC (Direct)	0.68/-	-	[90]
C ₄ N ₄	4.99	Square	-	SM	-/-	-	[117]
C ₅ N	3.65 (and 8.90)	Rectangular	-	M	-/-	-	[95]
C ₅ N ₂ (type - a, b and c)	6.41	Hexagonal	-	M	-/-	-	[97]
TPH-C ₅ N ₃	7.79 (and 6.05)	Rectangular	-	SM	-/-	-	[94]
C ₅ N ₄	7.19	Orthorhombic	-	SM	-/-	-	[91]
C ₆ N	7.19 (and 8.01)	Rectangular	1.71	SM	-/-	-	[118]
C ₆ N ₂	7.31 (and 5.76)	Rectangular	-	SM	-/-	-	[119]
C ₆ N ₃	11.07	Hexagonal	-	M	-/-	-	[120]
Dumbbell C ₆ N ₄	4.64	Hexagonal	2.04	SC (Direct)	0.80/-	-	[39]
C ₆ N ₆	7.12	Hexagonal	-	SC (Direct)	3.22/-	-	[48, 121, 3]
C ₆ N ₇	11.72	Hexagonal	-	SC (Direct)	1.97/2.09	Y (Thermal polymerisation)	[122, 123]
C ₇ N	10.0 (and 5.8)	Rectangular	-	M	-/-	-	[98]
Dumbbell C ₇ N ₂	4.89	Hexagonal	1.67	M	-/-	-	[39]
Dumbbell C ₇ N ₃	4.89	Hexagonal	2.02	BMS (Direct for ↑ and indirect for ↓)	0.90(↑) and 1.70(↓)-	-	[39]
C ₇ N ₃	8.69	Hexagonal	-	SM	-/-	-	[5]
C ₇ N ₆	6.79	Hexagonal	-	SC (Direct)	2.25/-	-	[124]
C ₇ N ₉	7.19	Hexagonal	-	SPM	-0.006	-	[105]
g-C ₈ N ₆	7.17	Hexagonal	-	SC (Indirect)	2.89/-	-	[125]
C ₈ N ₈	7.23	Tetragonal	-	M	-/-	-	[126]
Dumbbell C ₉ N	4.845	Hexagonal	1.72	M	-/-	-	[39]
C ₉ N ₄	6.875	Hexagonal	-	M	-/-	-	[99]
C ₉ N ₄	9.64	Hexagonal	-	SM	-/-	-	[92]
C ₉ N ₇	7.23	Hexagonal	-	HM (Direct)	0.29/0.46	-	[105]
C ₁₀ N ₃	6.948	Hexagonal	-	M	-/-	-	[99]
C ₁₀ N ₆	7.29	Hexagonal	-	HM (Direct)	1.52/2.72	-	[105]
C ₁₂ N	-	Hexagonal	-	SC (Direct)	0.62/0.98	-	[127]
C ₁₂ N ₂	7.985	Hexagonal	-	SC (Direct)	0.5/0.98	Y (Cross-coupling reaction/Interfacial synthesis)	[128]
C ₁₃ N ₃	10.61	Hexagonal	-	SM	-/-	-	[5]
C ₁₈ N ₆	16.038	Hexagonal	-	SC (Direct)	2.20/3.33	Y (Cross-coupling reaction/Interfacial synthesis)	[128]
C ₁₉ N ₃	12.22	Hexagonal	-	SM	-/-	-	[5]
C ₂₂ N ₄	8.52 (and 8.11)	Rectangular	-	SC (Quasi-direct)	1.14/-	-	[93]
C ₃₆ N ₆	18.664	Hexagonal	-	SC (Direct)	1.10/1.55	Y (Cross-coupling reaction/Interfacial synthesis)	[128]

Table 2: Table containing the basic details of different carbon nitride networks. Here SC, M, SPM, SM, DNL, HM, BMS stand for the semiconducting, metallic, spin-polarized metal, semi-metallic, Dirac nodal line, half-metallic and bipolar magnetic semiconducting electronic nature of the materials respectively.

Structure	a_0	Lattice mismatch (%)	Interlayer distance	Electronic nature (Type)	Bandgap (Theory/Expt.)	Synthesis (Method)	Reference
Bilayer C ₂ N	8.31	-	3.08	SC (Direct)	1.58/-	-	[129]
Bilayer TH-CN ₂	4.18 (and 5.78)	-	5.18-5.44	SC (Indirect)	4.48 and 4.53/-	-	[54]
Bilayer C ₃ N	7.12	-	3.30	SC (Indirect)	(0.30-1.21)/(0.40±0.04)-(0.85 ± 0.03)	Y (Hydrothermal)	[30]
Bilayer H-C ₃ N ₂	12.29	-	2.99-3.62	SC (Direct)	0.35-0.49	-	[68]
Bilayer T-C ₃ N ₂	8.63	-	2.71-3.40	SM and SC (Indirect)	(0.1-0.22)/-	-	[68]
Bilayer g-C ₃ N ₄	7.12	-	3.30	SC (Direct)	1.70/2.60	Y (Molecular composite precursors)	[130, 131]
Bilayer C ₉ N ₄	9.64	-	3.45	NC	-/-	-	[92]
C ₂ N/C ₃ N	8.41 (and 19.20)	-	Coplanar	M	-/-	-	[31]
C ₂ N/C ₆ N ₆	14.32	1.18	3.10	SC (Indirect)	2.00	-	[132]
g-C ₃ N ₄ /g-C ₆ N ₆	7.13	0.18	2.63	SC (Indirect)	2.60/-	-	[32]
g-C ₃ N ₄ /g-CN	7.10	0.8	3.41	SC (Indirect)	2.42/-	-	[133]
g-C ₃ N ₂ /g-CN	7.11	0.3	2.94 (and 3.42)	SC (Indirect)	0.86/-	-	[33]

Table 3: Table containing the basic details of carbon nitride bilayers and heterostructures. Here SC, M, SM, NC stand for the semiconducting, metallic, semi-metallic, nodal cylindrical electronic nature of the materials respectively.

ferent semiconductors, enabling the simultaneous reduction of protons to hydrogen and oxidation of water to oxygen. This mechanism is crucial for designing efficient photocatalytic systems for applications such as solar fuel production and environmental remediation as we have discussed in a later section of heterostructures. The combination of ultrathin carbon nitride nanostructures, strong interfacial interactions, and staggered band alignment has facilitated a Z-scheme pathway for efficient charge-carrier separation and transfer [135], achieving a solar-to-hydrogen efficiency of 1.16% under one-sun illumination. In 2015, Akple *et al.* reported the synthesis of WS₂-graphitic carbon nitride (g-C₃N₄) composites using WO₃ and thiourea as precursors in a gas–solid reaction. Varying amounts of WS₂ were loaded onto g-C₃N₄ to create heterostructures, which exhibited improved photocatalytic activity for H₂ production under visible light illumination [136]. In 2021, theoretical research demonstrated that an electric field is generated from the (C-doped) TiO₂ (101) surface toward the (B-doped) g-C₃N₄ monolayer in pristine, C-doped, and B-doped g-C₃N₄/TiO₂ heterostructures. Additionally, a higher band-edge potential was observed on the (C-doped) TiO₂ (101) surface compared to the (B-doped) g-C₃N₄ monolayer. Consequently, the pristine (2.591 eV), C-doped (2.663 eV), and B-doped (2.339 eV) g-C₃N₄/TiO₂ heterostructures were identified as Z-scheme systems, which enhance charge separation while preserving significant redox capabilities [137]. More recently, the exploration of potential systems based on two-dimensional (2D) heterostructures composed of carbon, nitrogen, or similar main group elements with special emphasis on the dynamics of excited charge carrier transfer and recombination processes is provided by Ghosh *et al.* [138], which are crucial for developing efficient photocatalytic systems for overall water splitting. A recent report shows a critical first-principle investigation of g-GeC/MoSe₂ van der Waals heterostructure which follows the Z-scheme photocatalytic mechanism and demonstrates enhanced light-harvesting efficiency across both the visible and ultraviolet wavelength ranges. In the same footing, a type-II vdW heterostructure of C₂N/C₆N₆ allows solar energy harvesting in the visible spectrum for water splitting [132]. As far as the experimental realizations are concerned, in 2013, Dong *et al.* developed a facile in-situ method to form a g-C₃N₄/g-C₃N₄ metal-free heterojunction with molecular composite precursors to facilitate the charge separation [131]. For the process, 6 gm of thiourea and 6 gm of urea were diffused with 30 mL water in an alumina crucible. The solution was dried at a temperature of 60°C overnight to

have the molecular composite precursors. These precursors in an alumina crucible were heated at 550 °C at a rate of 15°C per minute in a muffle furnace and kept for 2 hr. After the reaction, the alumina crucible was brought to room temperature and the resultant was collected for further utilization. An enhancement in the visible-light-absorption than a single layer is achieved by a bilayer g-C₃N₄, and the calculated optical absorption threshold is significantly shifted downward by 0.8 eV, which is reported to be induced by the interlayer coupling [29].

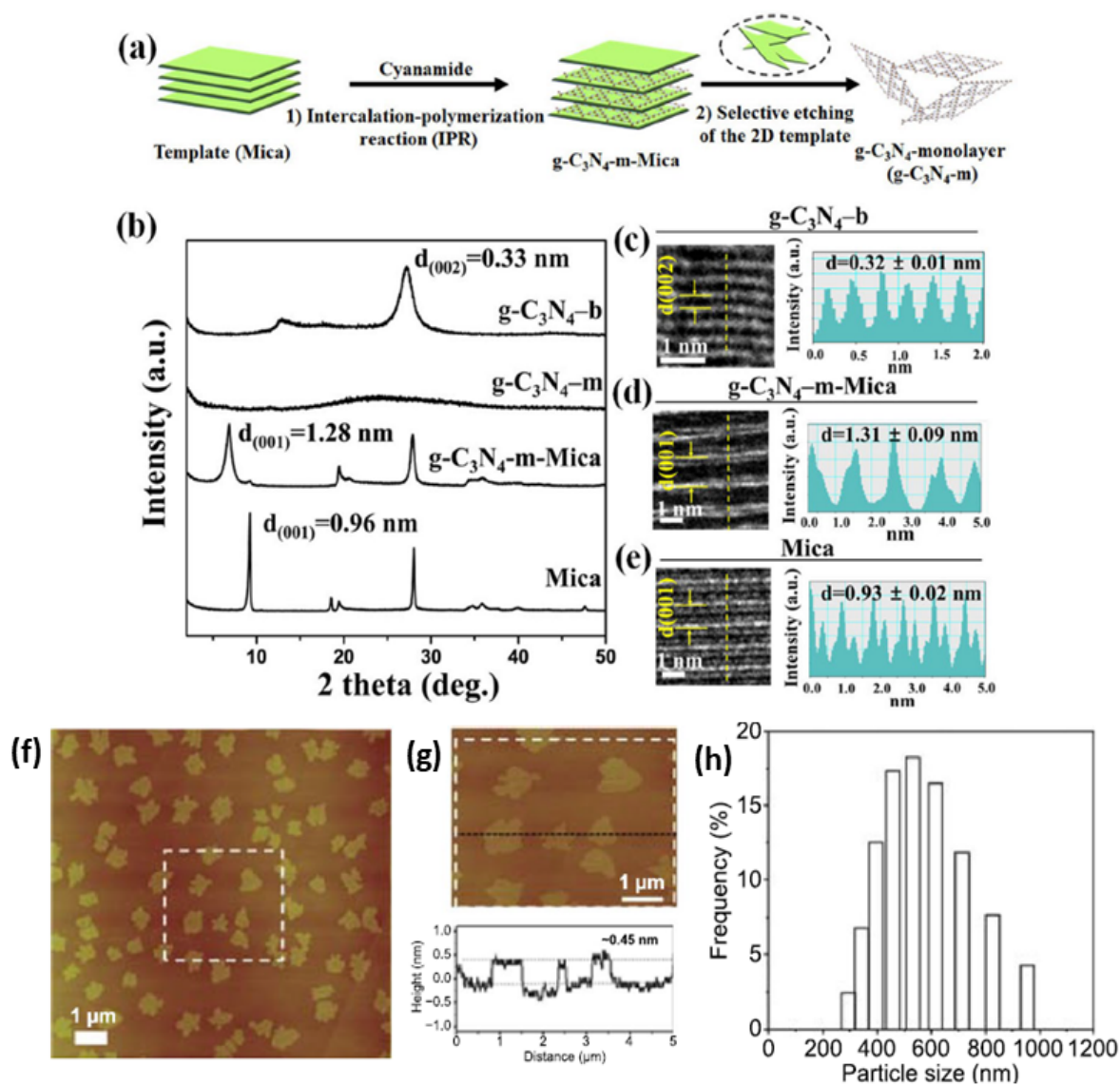


Figure 5: (a) Schematic diagram for the synthesis of g-C₃N₄-m by using the 2D Mica template. (b) XRD patterns of Mica, g-C₃N₄-m-Mica, g-C₃N₄-m and g-C₃N₄-b. (c-e) Cross-sectional HRTEM images and photometric intensity profiles along the yellow dashed lines for g-C₃N₄-b, g-C₃N₄-m-Mica and Mica. **AFM image of g-C₃N₄-m.** (f) The g-C₃N₄-m monolayers dispersed on the freshly-cleaved muscovite mica substrate. (g) The thickness of g-C₃N₄-m monolayer flakes, and the height profile along the black dashed line. (h) The histogram for the size distribution of g-C₃N₄-m. Reproduced with permission from Springer Nature (2022).

In 2021, Wei *et al.* reported the successful synthesis of C_3N bilayers where different proportions of 2,3-diaminophenazine (DAP) precursor and time were used to grow these structures [30]. The stacking orders can be tuned effectively by changing the reaction time of the hydrothermal treatment of DAP, and a higher growth time results in the formation of AA' (and AB') stackings. The DAP aqueous solution of 300.0 mL and 3.0 mM (200.0 mL, 2.0 mM) was added into a 100 mL PPL-lined stainless steel autoclave, heated at 200°C for 72 hr (and 192 hr). The products were separated by centrifugation with the specifics of 10000 r per minute, 60 min, 10°C. The electronic bandgap of 0.40 ± 0.04 eV (and 0.85 ± 0.03 eV) was obtained for C_3N bilayer with AA' (and AB') stacking - determined through a statistical analysis of 30 individual STS curves obtained on multiple bilayer samples. Interestingly, a new structure of nodal line, i.e., nodal cylinder, is found in momentum space for AA-stacking C_9N_4 [92]. Table-3 here provides all the existing C_xN_y hetero-bilayers with necessary details and references.

3. Automation in material science

Material science research has shown a paradigm shift whence the automated discovering of crystal structure was introduced. Different crystal search algorithms were proposed over time like particle swarm optimization in CALYPSO [139] and other metaheuristic algorithms [140], evolutionary algorithm in USPEX [141, 142], simulated annealing in Sir2019 [143], EXPO2014 [144], metadynamics [145, 146], and many others. Sometimes, a simple method such as an automated neighbour finding approach relying on the idea that increased covalent bonding nature within local substructure increases the stability may be proved enough for finding out new CN like structures [147]. With their merits and limitations these high-throughput studies can generate huge data on crystal structures and investigate their viability through stability check spanning all over the crystallographic space.

The application of ML in structure prediction is a relatively recent advancement. A ML based prediction and analysis framework, incorporating a symmetry based combinatorial crystal optimization program (SCCOP) and a feature additive attribution model, was developed to significantly reduce computational costs and extract property-related structural features [148]. This approach was demonstrated practically on a 2D B-C-N system, showcasing its capability for high-throughput structural search and feature extraction. Initially, structures generated from 17 plane space groups were converted into crystal vectors using a graph neural network (GNN), followed by energy prediction. Bayesian optimization was employed to explore the structure's potential energy surface minimum. Subsequently, desired structures were optimized using ML-accelerated simulated annealing (SA), supplemented by a limited number of DFT calculations to achieve the lowest energy configuration.

Prediction of materials properties associated with the formation and stability such as formation enthalpy [149, 150], phononic dispersion [151, 152] with at par accuracy of quantum mechanics calculations and much lower computational cost is becoming popular with time.

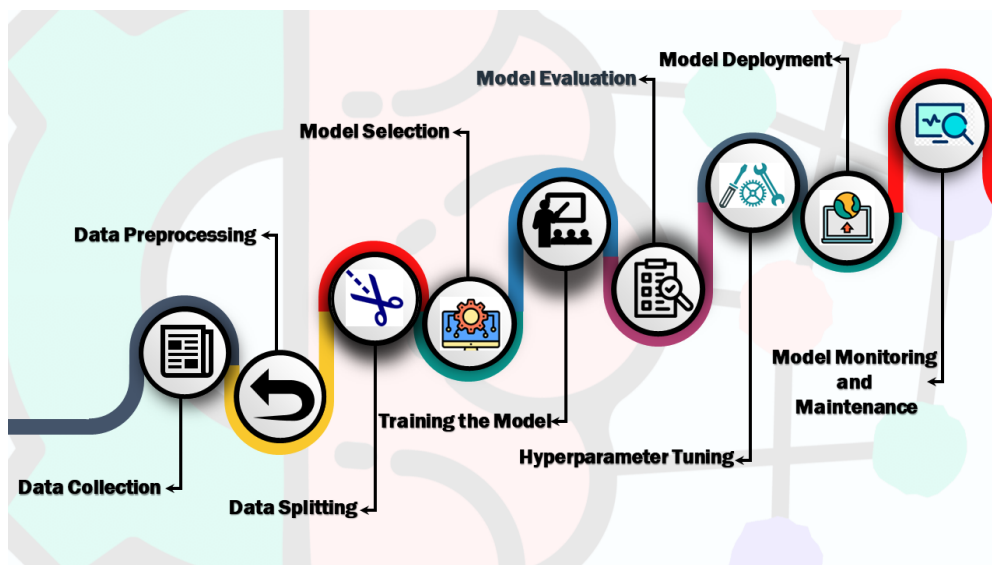


Figure 6: Different steps in Machine Learning process

4. The Machine Learning Modelling

The key of Machine Learning is data. Larger the dataset is, precise the predictions are. In human idea, gathering data is like gathering experiences. The standard of dataset depends on the volume as well as on the versatility. In material science the volume of data is increasing day by day due to the automated high-throughput discovery of materials properties. Different platforms as tabulated in Table-4 are readily available for throughput calculation. Datasets ideally have some input parameters and the corresponding outputs. The next step in ML algorithm is finding relevant input descriptors those can be mapped to the outputs. This step is called featurisation. Once the featurisation completed, a suitable ML model is built mapping the descriptors to the output. Then the model is tested to evaluate its predictive power. A brief description of the steps (see Figure-6) follows:

4.1. Data collection and curation

Collecting data is the very first step in ML. Materials' data can be acquired either from experimental or from theoretical studies. Different databases are maintained, some of those are listed in Table-5. Now, the experiments are done in different conditions or the methods for characterising properties differ, so, differences in results is ubiquitous. If the data is checked before entering in databases, this variation remains. Similar situation is observed for computational data due to methodological variation. Besides the available databases, data can be acquired directly from the research articles through natural language processing, however, quality checking through human intervention is highly required till now.

Data collected from different sources may incur confusion. Data curation is an essential step to manage and maintain the data. It helps to improve the quality of the data through cleaning, inconsistency correction, and removing duplicate entries. In some cases the database may have some missing entries those are addressed in this step as well.

4.2. Featurisation

The data has to be presented in a mathematical form understandable by computers. This involves expressing the characters of materials and its constituents (atoms, molecules, ligands, etc.) by numerical values. For example, in any solid formed by different elements, the mass number, number of electrons, valence electronic configuration, crystal structure, symmetries, coordination number of the atoms, etc. can be treated as the fingerprints or descriptors. These descriptors should be unique from each other and the number of descriptors should be optimum, not so much that the model overfits or not so less that the vital parameters are left aside. There are chances of having different descriptors with high correlation or descriptor with almost same value throughout. Feature selection is a technique to reduce the dimensionality of input parameters so that a smaller subset of the relevant features can be extracted through the removal of redundant, irrelevant, or noisy descriptors. This is done using different supervised or unsupervised techniques:

4.2.1. Supervised techniques

In case of supervised learning the input data are labelled, which means every element is tagged with a correct classification. For example, if a number of figures of cubic and orthorhombic unit cells are provided and each of those are classified then the data is labelled. From this data, the machine may learn to identify a unit cell not in this dataset as cubic or orthorhombic. So, from the initial point the labelling is output oriented. Supervised techniques of feature selection are broadly put into three categories: filter based, wrapper based and embedded approaches.

In filter based strategy the correlation of data with each other is evaluated not considering the ML model to be used. This can be as simple of seeing the importance (importance score) of all the features by sorting, categorised as information-gain method. Another widely used technique is chi-squared-test which is a simple statistical tool to evaluate the correlation of different entities. Method using Fisher's criteria to rank the variables in descending order for determining most interesting feature is another widely used technique. If there are many missing values of any parameter that descriptor should be dropped. This is done by calculating the missing value ratio which is the number associated with each column found by the ratio of total number of missing values and the total number of observations.

The wrapper based method utilises specific machine learning to determine the best combination of features through evaluation and comparison with other combinations. On the basis of performance, descriptors are added starting from an empty set (forward selection) or subtracted from the set of all descriptors (backward selection), and in every step the model is trained again. Both of these are serial methods, so, all combinations are not tested. Exhaustive selection method evaluates all possible subsets of features to identify the best performer.

While there is no option of learning in filter methods, wrapper methods use separate learning algorithm for feature selection. In embedded method the feature selection embeds with the ML model algorithm itself and feature selection part can not be separated from the learning part. These are faster than wrapper based methods as the ML model is fitted only once. In regularisation technique a penalty term is added to the coefficients of different features so that for some of those the coefficients become zero, hence, the overfitting of the model can be avoided. On the other hand,

decision tree based methods Random-forest or Gradient-boosting look at the outcomes from all the different nodes of decision trees. Through the tree building process, significance score for all the features are computed and thus sorted.

4.2.2. Unsupervised techniques

Where supervised learning is goal oriented, unsupervised strategies use algorithms to find correlation in data without any explicit instruction. This works with unlabelled data. Principal component analysis is such a strategy that transforms the original correlated features into a set of orthogonal features while conserving the variance as much as possible. These principal components are essentially linear combinations of the original descriptors. Independent component analysis is a linear transformation method targeting the statistical independence of features as good as possible. Two random variables are statistically independent if the joint probability can be expressed as the multiplication of individual probabilities. Beside these, there are other strategies with higher complexity like Non-negative matrix factorization, Autoencoders, etc.

4.3. Splitting data in training, validation and test subset

This is one of the crucial steps for ML before selection of model. The model is fit on a dataset called training dataset. The fitted model is then used to predict outputs on a second dataset named as the validation dataset to provide an unbiased evaluation of the trained model. The hyperparameters of the model is tuned depending on this evaluation and a final model is prepared. Finally, test dataset is used to evaluate the performance of the final model.

The simplest method to split the data is Random splitting which divides the dataset randomly into these three types. Random splitting works well on balanced data where all the types have enough examples in the dataset. For imbalanced datasets, to ensure the consistency in class distribution among subsets, stratified splitting technique is used. Now for sequential data (time-series data) random sampling can be chaotic, so, time-series splitting preserves the temporal order of data. All of these are one-shot methods. Cross validation method like K-fold cross validation produces “k” equally sized subset from the dataset. In each of k-step iteration, one of these work as a validation subset and the other (k-1) subsets as training subsets. For small dataset Leave-one-out cross validation is an effective method. At an iteration step, one sample is taken as a test sample, and the remaining samples form the training set. The iteration is repeated for every sample. In cross validation methods the evaluation results are averaged over the number of iterations to evaluate the performance of ML model.

4.4. Model selection and training

This the most important part. Choice of ML model is very much problem dependent as well as performance oriented. The ML models are broadly classified in three classes (see, Figure-7):

- Supervised learning
- Unsupervised learning

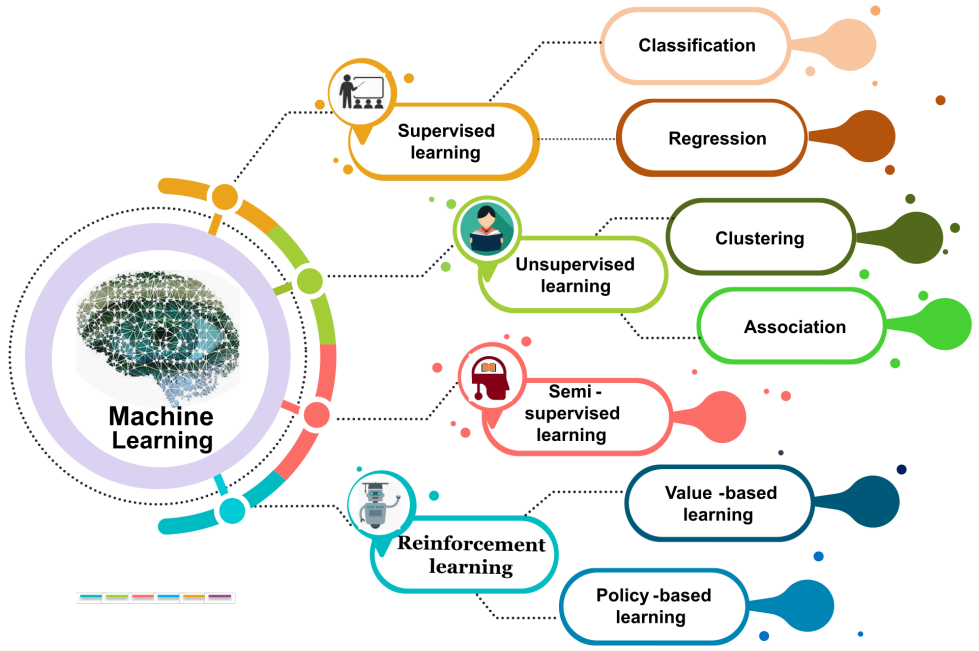


Figure 7: Classification of Machine Learning models

- Reinforcement learning

To estimate how well a particular ML model performs, loss function is calculated. Different loss functions are used:

- Mean Squared Error (MSE):

$$MSE = \frac{1}{n} \sum_i^n (y_i - \hat{y}_i)^2$$

where, \hat{y}_i and y_i are the original and predicted output values.

- Mean Absolute Error (MAE):

$$MAE = \frac{1}{n} \sum_i^n |y_i - \hat{y}_i|$$

- Huber Loss: Hybrids MSE and MAE in single loss function:

$$L_{\delta,i}(\hat{y}_i, y_i) = \begin{cases} \frac{1}{2}(\hat{y}_i - y_i)^2 & \text{if } |\hat{y}_i - y_i| \leq \delta \\ \delta(|\hat{y}_i - y_i| - \frac{\delta}{2}) & \text{otherwise} \end{cases}$$

- Hinge loss: This is another loss function for binary classification, where, two classes of data points labelled as +1 and -1 are meant to be separated.

$$L_i = \max[0, (1 - \hat{y}_i) \cdot y_i]$$

where, \hat{y}_i is the actual class (-1/1) and y_i is the classifier predicted value for the data point.

- Binary cross entropy loss/ Log loss: For classification problem the question arises, whether the output is this (let, put numerical value $y = 1$ for YES) or not ($y = 0$ for NOT). If $p(y_i)$ is the probability of finding YES at any data point i then

$$L = -\frac{1}{n} \sum_i^n [y_i \cdot \log(p(y_i)) + (1 - y_i) \cdot \log(1 - p(y_i))]$$

- The coefficient of determination: The coefficient of determination, R^2 , is a statistical measure that indicates how well the regression predictions approximate the real data points. It is defined as:

$$R^2 = 1 - \frac{SS_{\text{res}}}{SS_{\text{tot}}}$$

where SS_{res} is the sum of squares of residuals (the differences between the observed and predicted values) and SS_{tot} is the total sum of squares (the sum of squared differences between the observed values and their mean). R^2 ranges from 0 to 1, where, $R^2 = 1$ indicates that the model perfectly predicts the dependent variable using the independent variables, and $R^2 = 0$ indicates that the model does not explain any of the variance in the dependent variable around its mean.

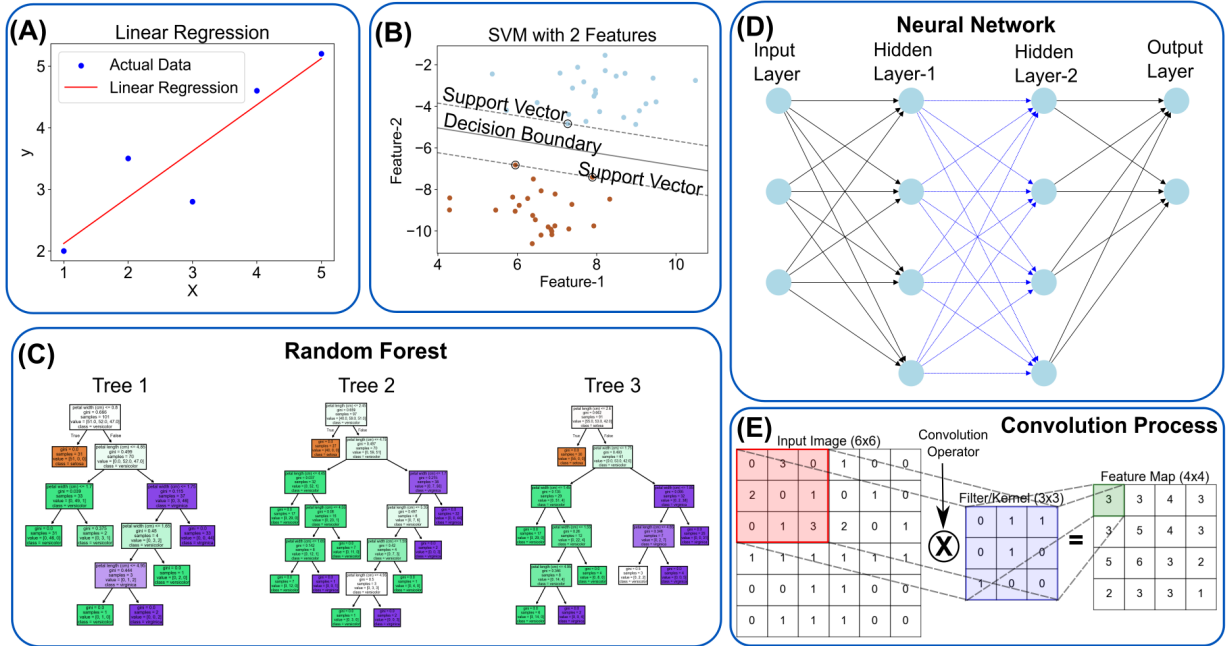


Figure 8: Different Machine Learning models. Linear Regression, Support Vector Machine with two features. A Random Forest with three decision-trees. Artificial Neural Network with more than one hidden layers identified as Deep Neural Network and the convolution process, precursor to Neural Network in convolutional Neural Network.

4.4.1. Supervised ML models

As discussed earlier supervised technique works with labeled data and essentially goal oriented. Further subdivisions of supervised learning are: Classification and Regression.

In regression, the output parameter is a continuous variable, while classification outputs discrete variables. For example, categorizing solids as metals or insulators is a classification problem, whereas, predicting the bandgap of any solid from different input variables is a regression problem.

Regression:

Regression analysis is a statistical method used to model the relationship between one or more independent variables and a dependent variable. It seeks to identify and quantify the impact of these variables on the outcome, facilitating prediction and understanding of the underlying data patterns. There are numerous types of regression methods used in ML (see, Table- 5 for their strong and weak points), for example:

- *Linear Regression (LR)*: The linear relationship between the dependent output variable (y) and one or more independent input features (x 's) by fitting a straight line $y = \sum_i m_i x_i + c$ is established through this simplest type of regression method.
- *Multiple Linear Regression (MLR)*: Multiple Linear Regression (MLR) is a statistical method used to model the relationship between multiple independent variables and a continuous dependent variable. It assumes a linear relationship between predictors and the target variable, making it straightforward to interpret. MLR estimates the coefficients of each variable to minimize the sum of squared differences between predicted and observed values. While simple and efficient, MLR may struggle with non-linear relationships and interactions between predictors.
- *k-Nearest Neighbors Regression (KNN)*: It is a non-parametric machine learning algorithm used for regression tasks. It predicts the value of a new data point by averaging the values of its k nearest neighbors in the training dataset. The ' k ' in KNN represents the number of neighbors considered for prediction, which is typically chosen based on cross-validation or other model selection techniques. KNN does not make any assumptions about the underlying data distribution and can capture complex relationships between input and output variables. However, its performance can be sensitive to the choice of k and the distance metric used to measure similarity between data points.
- *Ridge Regression (RR)*: Ridge Regression is a linear regression technique that incorporates regularization to address multicollinearity and improve model generalization. It adds a penalty term to the standard least squares objective function, which is proportional to the square of the magnitude of the coefficients. This penalty term (controlled by a regularization parameter, typically denoted as α) shrinks the coefficients towards zero, effectively reducing their variance and mitigating the influence of correlated predictors. RR is particularly useful when the number of predictors (features) is large, or when predictors are highly correlated. By imposing regularization, RR helps to stabilize the model and improve its performance on new, unseen data. The optimal value of α is usually determined through cross validation.

- *Kernel Ridge Regression (KRR)*: It is a supervised learning algorithm used for regression tasks. It extends RR by using the kernel trick, which allows it to handle non linear relationships between input variables and the target variable. KRR minimizes a regularized objective function that includes both the squared error loss and a penalty term that encourages smoothness in the predictions. The choice of kernel function (such as linear, polynomial, Gaussian radial basis function, etc.) determines the type of non-linear transformation applied to the data. KRR is particularly useful when the relationship between input and output variables is complex and cannot be effectively modeled by linear regression. However, it requires tuning of hyperparameters such as the regularization parameter and the kernel parameters to achieve optimal performance.
- *Gradient Boosting Regression (GBR)*: Gradient Boosting Regression (GBR) is an ensemble learning technique that sequentially combines weak learners, typically decision trees, to build a predictive model. It works by fitting new models to the residuals of the previous predictions, thereby minimizing the error. GBR is known for its ability to capture complex interactions and non-linear relationships in data, making it a powerful tool for predictive modeling. However, it can be computationally intensive and prone to overfitting if not carefully tuned.
- *Extreme Gradient Boosting Regression (XGBoost)*: Extreme Gradient Boosting Regression (XGBoost) is an advanced implementation of gradient boosting (GBR) that has gained popularity for its speed and performance. It uses a regularized objective function and parallel computing to optimize model training and prediction. XGBoost excels in handling large datasets, missing values, and complex interactions between variables. Despite its effectiveness, XGBoost may require careful tuning of parameters to prevent overfitting and achieve optimal performance.
- *Support Vector Regression (SVR)*: Support Vector Regression (SVR) is a regression technique based on Support Vector Machines (SVMs), which find the optimal hyperplane that best fits the data while minimizing prediction errors. SVR is particularly effective in high dimensional spaces and can handle non linear relationships through the use of kernel functions. However, SVR's performance heavily depends on the choice of kernel and regularization parameters, which can be challenging to optimize. It is also sensitive to outliers in the data, requiring careful preprocessing steps.
- *Least Absolute Shrinkage and Selection Operator (LASSO)*: LASSO regression is a linear regression technique that incorporates regularization to improve the model's prediction accuracy and interpretability. It penalizes the absolute size of the regression coefficients, forcing some coefficients to shrink towards zero. This encourages sparsity and feature selection, making Lasso particularly useful when dealing with datasets with many correlated variables or when aiming to identify the most important predictors. Adjusting the regularization parameter allows for control over the degree of regularization applied, balancing model complexity and predictive performance.

Decision Trees (Classification/Regression)

A decision tree is a flowchart like tree structure. It is used to make predictions or decisions. In this tree structure the nodes represent tests, branches represent the different outcomes, and leaf nodes represent the predictions.

Random Forests (Classification/Regression)

In Random Forest (RF) strategy multiple decision trees are built to reach a single result. This is an ensemble method made up of a set of these trees and their predictions are aggregated to recognize the result with majority of votes.

Extra-Trees (Classification/Regression)

Extra Trees, or Extremely Randomized Trees, is an ensemble learning method based on decision trees, similar to RFs but with additional randomness in the selection of splitting points. This approach further diversifies the trees by selecting random thresholds for node splitting, aiming to improve generalization and robustness by reducing variance and potential overfitting in regression tasks.

Support Vector Machine(Classification)

Support Vector Machine is used mostly for linear or non-linear classification, however, it is also used for regression. The objective of SVM is to determine the optimal hyperplane that can isolate the data points in separate classes. If there are two distinct classes, the hyperplane is just a line, for three classes two planes can separate. In general, in SVM model a data point is viewed as a n-dimensional vector and it tries to find a (n-1) dimensional hyperplane to separate those points. Though the original proposal was a linear hyperplane, later non-linear SVM was proposed [153].

Naïve Baye's(Classification)

The Baye's theorem on conditional probability is expressed as

$$P(A|B) = \frac{P(B|A)P(A)}{P(B)}$$

where, $P(A|B)$ is the conditional probability of event—A when event—B is true, $P(B|A)$ is the conditional probability of event—B when event—A is true, and $P(A)$, $P(B)$ are the probabilities of A and B without any given condition. For a class variable y and dependent features x_i 's, this looks like

$$P(y|x_1, x_2, \dots, x_n) = \frac{P(x_1, x_2, \dots, x_n|y)P(y)}{P(x_1, x_2, \dots, x_n)}$$

Now, the "naive" conditional independence approximation assumes that all the features are mutually independent, so that:

$$P(x_i|y, x_1, x_2, \dots, x_{i-1}, x_{i+1}, \dots, x_n) = P(x_i|y)$$

$$\Rightarrow P(y|x_1, x_2, \dots, x_n) = \frac{P(y) \prod_{i=1}^n P(x_i|y)}{P(x_1, x_2, \dots, x_n)}$$

For a given set classes, the classification output is found simply as:

$$y = \arg \max_k P(y_k) \prod_{i=1}^n P(x_i|y_k)$$

There are different types of naive Baye's algorithm: Gaussian naive Baye's, Multinomial naive Baye's, Bernoulli naive Baye's, etc.

Gaussian Process Regression (GPR)

Gaussian Process Regression (GPR) is a probabilistic supervised learning method used for regression tasks. It models the relationship between input variables and the target variable as a Gaussian process, which is a collection of random variables indexed by the input space. GPR assumes a prior over functions, typically Gaussian, and updates this prior based on observed data to obtain a posterior distribution over functions that best fit the data. Predictions are made by computing the mean and variance (or uncertainty) of the posterior distribution at new input points. GPR is flexible in capturing complex patterns in data without assuming a specific functional form, making it suitable for tasks where the underlying relationship is not well understood or may exhibit non-linearities. However, its computational complexity increases with the size of the dataset, requiring efficient approximation methods for scalability.

Artificial Neural Networks:

In brain, neurons have very complex network. The dendrites of neurons take the input and axon transfer the output to other neurons (see Figure-8). Synapses handle the transmission of nervous impulses between neurons or neurons to cells. Motivated by this, the artificial neural networks (ANN) have input nodes, output nodes and weights to tune the transmission of data from output nodes to input nodes of other neurons. In ANN there is an input layer, an output layer and one or more hidden layers in between.

The most basic ANN is unidirectional feedforward neural network. The data enters through the input layer and go out through the output layer,. The hidden layers between input and output may or may not exist. Through the backpropagation technique the weights between nodes can be adjusted depending on the error calculation. A comprehensive list of different ANN architectures, their strong and weak points are tabulated in Table-6.

If a series of layers is used in feedforward ANN, then generally it is called Deep Learning. In deep neural network (DNN) the useful feature are automatically extracted from the data. It can model non-linear relationships as well.

In mathematics convolution is defined as a way of combining two functions into third function. In convolutional ANN (CNN) a set of learnable filters is used on data to to extract features. This is done convolution layer as depicted in Figure-8. This is essentially a DNN.

A feedback neural network allows signals to use feedback paths for travelling in both directions. This type of network contains loops, thus a nonlinear dynamical system is produced. Recurrent neural network (RNN) is a prominent

variety of feedback neural network. RNNs are designed for sequential data processing, capable of capturing dependencies and patterns over time through recurrent connections. They are widely used in tasks such as natural language processing, time series prediction, and speech recognition, where temporal dynamics play a crucial role.

General Regression Neural Networks (GRNN) are a type of neural network architecture utilized primarily for regression tasks. They employ radial basis functions in their hidden layer neurons to approximate continuous functions based on input data. GRNNs are known for their capability to model complex and nonlinear relationships between input and output variables effectively. Unlike traditional neural networks, GRNNs adopt a memory based learning approach, storing all training samples in memory for rapid prediction during inference. This architecture makes GRNNs suitable for applications requiring accurate regression predictions, where the underlying data relationships are intricate and may not conform to linear patterns.

Activation functions: Activation functions are crucial components in artificial neural networks, responsible for introducing non-linearity into the network's output. They operate on the weighted sum of inputs to a neuron and determine its output. Each activation function serves a specific purpose, facilitating the network's ability to model complex relationships within data.

The linear activation function, denoted as `purelin`, is defined as:

$$\text{purelin}(x) = x$$

This activation function simply outputs the input x without applying any transformation. It is typically used in the output layer of neural networks for regression tasks, where the network needs to predict continuous values. Purelin preserves the linearity of the input data and produces outputs that are directly proportional to the input, making it straightforward for interpretation and computation in regression scenarios.

The logistic sigmoid activation function, often referred to as `logsig`, is defined as:

$$\text{logsig}(x) = \frac{1}{1 + e^{-x}}$$

It maps the input x to a value between 0 and 1, making it suitable for binary classification tasks or as a squashing function to normalize outputs in neural networks. This activation introduces non-linearity, enabling the network to learn complex patterns in the data by transforming the input into a probability-like output.

Additionally, the rectified linear unit (ReLU) is popular for hidden layers due to its computational efficiency and ability to handle vanishing gradient problems.

4.4.2. Unsupervised ML models

Unsupervised learning works with unlabeled data. Generally, three types of jobs are done using unsupervised learning:

- **Clustering:** It is a method of grouping the data based on the similarities. Segmentation of data into different groups enables analysis on each of those datasets to identify the inherent patterns.

- Dimension reduction: The number of features is called the dimensionality. For address overfitting issue and reduce the unneeded complexity of the model, dimension reduction is done.
- Association rule learning: The dependency of one item on another in a dataset is determined to identify the relations among variables so that any indication can be extracted. For example, if there are data on bandgaps and work functions or HOMO-LUMO positions in a dataset, it is likely that the article is targeted to find the catalytic merit of the material.

4.4.3. Reinforcement Learning

While in supervised learning labelled data is needed, reinforcement learning doesn't need that. Even it doesn't use unlabelled dataset as needed in unsupervised learning. It learns by its experience through the feedbacks and not intended in discovering a relationship in a dataset. Through trial and error, it tunes itself in accordance to the environment, thus creates new datasets in each trial. As, deep learning method uses unstructured data, it is natural for almost all reinforcement learning strategies to use ANN in some extent. Depending on approach, the reinforcement learning can be categorised in two sub-categories:

- Value based learning: The value based methods are meant to learn an optimal value function. The future reward of taking a step is anticipated for the present state.
- Policy based learning: The policy based methods are meant to learn an optimal policy directly. The model is built and updated without calculating any value function.

5. Generative Artificial Intelligence

While traditional ML models perform predefined tasks generative artificial intelligence (GAI) is a branch intended to generate new contents autonomously. Autoencoders emerged as the earliest form of generative models. Autoencoder is a type of ANN capable of learning network that is trained to compress input data effectively and regenerate it as output in unsupervised way. Variational autoencoders (VAE) introduced probabilistic modelling to autoencoders which allowed more flexibility in generating diverse outputs. Generative adversarial networks (GAN) revolutionized GAI by introducing a game-theoretical approach which resulted in highly realistic outputs. Both of these are very recent developments came after 2010. The timeline of the development of GAI is presented in Figure–9.

5.1. Variational Autoencoders

VAEs combine probabilistic modelling approach with ANN to represent complex dataset a lower-dimensional latent space. VAEs are applied in different generative tasks like image generation or natural language processing where generating novel and realistic data points is crucial.

Components

The different components of VAE are:

- **Encoder:** The encoder maps input data points to a probabilistic distribution in the latent vector space. The input can be an image, or text sequence, or, similar unlabelled data.
- **Latent space:** The latent space is a vector space having dimension lower than the original input data depending on different encoding techniques. VAEs apply a probabilistic structure to it so that meaningful sampling and interpolation between points can be done.
- **Decoder:** The decoder takes information from the latent space and reconstructs an output that resembles the original input. By probabilistic sampling from the latent space VAEs can generate data points similar but not identical to the original data. This regeneration process makes VAE a powerful tools for generative tasks.

5.2. Generative adversarial networks

GAN is made up of two ANNs, a discriminator and a generator. As training progresses, the generator improves its ability to produce more realistic data, guided by the feedback from the discriminator. Conversely, the discriminator also improves over time, becoming more adept at distinguishing real from fake data.

- **Generator:** The generator generates artificial data that resembles the input data. As input GAN takes latent vector or simply random noise. Its goal is to fool the discriminator by generating synthetic data indistinguishable from real data.
- **Discriminator:** The discriminator evaluates whether a given data is real (from input) or fake (synthetic). Distinguishing between real and produced data is essentially a binary classification task.

The two components of GAN, the generator and discriminator, are trained in parallel and are intended to compete. Initially, the discriminator easily identifies the random noise generated by the generator as fake. With iterations, both the generator and the discriminator improve by taking competitor feedback. The training process continues until an equilibrium is reached where the generator can generate synthetic outputs that are realistic enough to fool the discriminator.

6. Application of ML

While the research on CNs and other catalysts are prolific the application of ML in this field is relatively new. ML offers a promising alternative to accelerate the discovery of new materials and can provide pathway to enhance the performance of the traditional photocatalysts. From data curation to model selection and even to the generative AI regime a handful of works on catalysts, especially on CNs are found in literature.

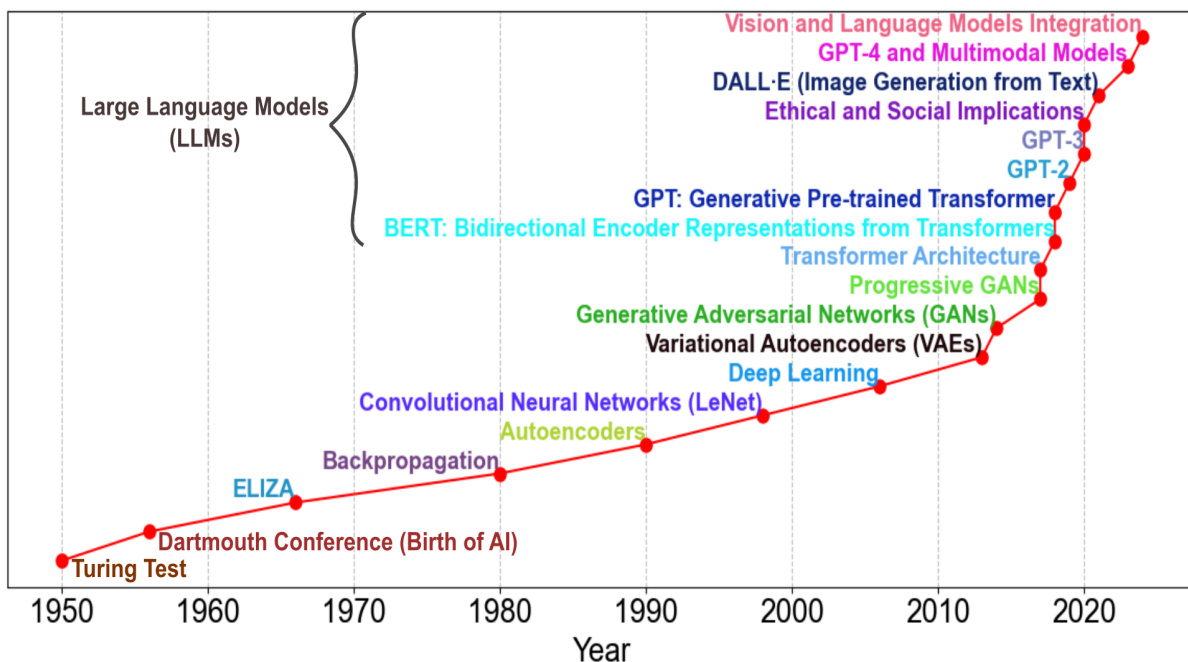


Figure 9: Timeline of Generative AI

Large datasets are built on experimental and theoretical findings for ML application over time. Most of the online repositories of materials' data and tools for ML application are presented in Table-6. A separate Table-7 is compiled dedicated to the online platforms for catalysts present. Through analysis of material properties, and performance metrics on large dataset, ML algorithms can identify patterns and correlations easily which demands much experience otherwise.

While data curation is the essential first step in ML modelling, ethical considerations are also important. This includes adherence to legal and ethical guidelines on data privacy, version control, and proper documentation for reproducibility and transparency of results.

Throughout the synthesis processes and diverse applications of CNs, the pervasive integration of ML is evident. Liquid-phase exfoliation (LPE) stands as the preeminent technique for synthesizing 2D $g-C_3N_4$ nanosheets. Key parameters assessing solvent efficacy in LPE include the free energy necessary (G_{exf}) to exfoliate a unit area of layered materials into individual sheets and the solvation free energy per unit area of a nanosheet (G_{sol}). ML algorithms were employed to predict G_{exf} and G_{sol} for $g-C_3N_4$, leveraging a database derived from MD simulations encompassing 49 distinct solvents with diverse chemical structures and properties [44]. Among the six ML methods investigated, the Extra-Tree regressor emerged as the optimal performer.

Band-gap modulation through doping of $g-C_3N_4$ represents a widely adopted technique. Modelling to predict band-gaps of doped $g-C_3N_4$ involved the utilization of experimental data derived from 105 $g-C_3N_4$ based compounds [45]. The low correlation coefficient observed between surface area and bandgap in doped $g-C_3N_4$ indicated that the

descriptor and target variables are not linearly correlated. Finally, the bandgap predictions from the SVR model perfectly aligned with experimental data points.

6.1. Machine Learned Potentials

One of the active field on theoretical material science is the development of machine-learning interatomic potentials (MLIP). While, classical force fields (e.g., Lennard-Jones) were handcrafted based on physical intuition and experimental data, MLIPs are generated using modelling on large simulated datasets. For example, CHGNet and M3GNet MLIP models are trained on Material Project database [154, 155]. Depending on the descriptors, MLIPs can be broadly categorized into two classes: those that rely on local descriptors and those that use graph-based descriptors. Local descriptors are computationally efficient and scalable, but they may not be able to capture long-range interactions. On the other hand, graph-based descriptors provide higher accuracy by modeling global atomic relationships considering entire structures, however complex they are. However, they are more computationally demanding and harder to interpret due to their complex nature, especially when using deep learning models are employed. A comprehensive description on the development of different MLIPs can be found in [156]. From Behler and Parrinello’s local descriptors based MLIP to recent developments on high-order tensor message passing interatomic potential have been discussed [157, 158]. Different use of MLIP on catalysis research is compiled by Choung *et al.* [159].

The utilization of MLIP has significantly advanced computational studies in materials science, particularly in predicting complex properties such as phononic dispersion, thermal conductivity, and mechanical responses in various CN based materials. Shapeev *et al.* . pioneered the development of moment tensor interatomic potentials using active learning methods under classical or ab-initio molecular dynamics (AIMD) data, enabling accurate calculations of phononic responses, as highlighted in Novikov *et al.* [160]. This approach was further applied to investigate the phononic dispersion and stress-strain relationships in C_6N_7 based 2D monolayers by Mortazavi *et al.* [161], and to study thermal expansion in complex nanomembranes [162]. The versatility of MLIP extends to various 2D CNs including C_3N_4 , C_3N_5 , and C_3N_6 , demonstrating its effectiveness in understanding the thermal and mechanical behaviors of these materials [163, 113]. Moreover, MLIP was successfully employed in non-equilibrium MD simulations on C_2N to predict lattice thermal conductivity and mechanical properties, illustrating its capability to simulate dynamic material responses under non-equilibrium conditions as detailed by Arabha *et al.* [164].

ML force fields have become increasingly prevalent in MD simulations, particularly in applications requiring extended timescales and complex phenomena such as tautomerism in materials like dual defect-modified g- C_3N_4 . Agrawal *et al.* utilized nonadiabatic MD simulations employing MLP to investigate tautomerism, a phenomenon where molecules exist in equilibrium between different structural isomers, which is challenging to capture with traditional AIMD methods limited to short timescales (picoseconds). This approach leverages MLPs to approximate interatomic potentials more accurately over longer simulation times, allowing researchers to study dynamic processes like tautomerism in detail. The study exemplifies the utility of ML based approaches in overcoming the temporal and computational limitations of AIMD, thereby advancing our understanding of complex molecular behaviors in

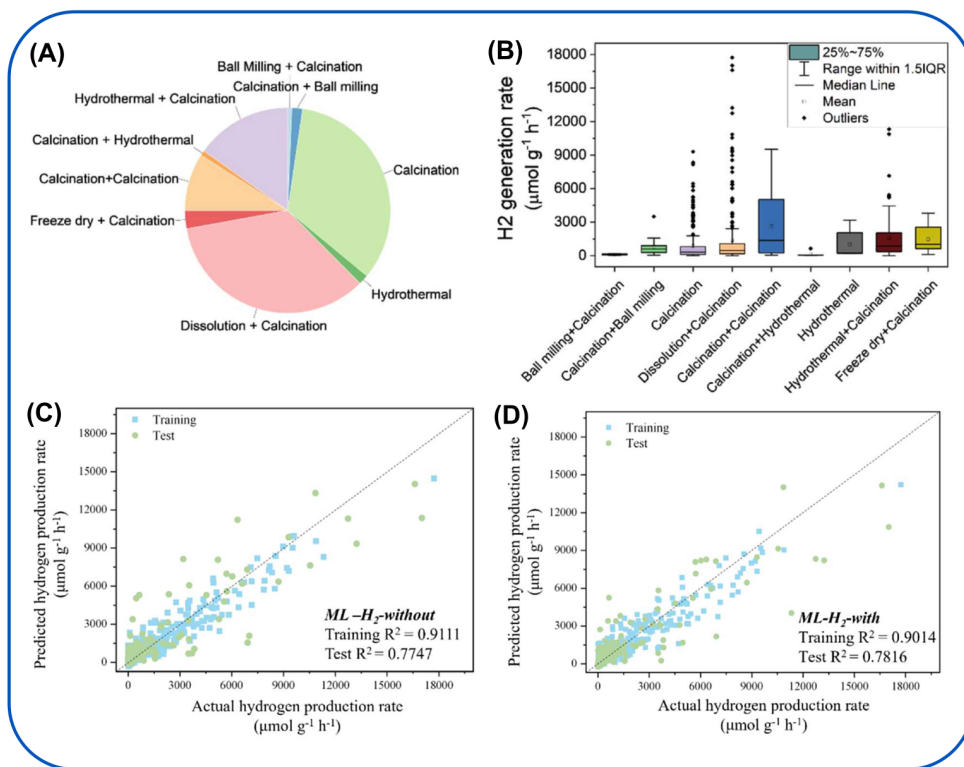


Figure 10: (A) Frequency distribution of each synthesis method within the datasets. (B) H₂ production rates categorized by treatment methods. (C) and (D) Machine learning model performance metrics for predicting H₂ production rates without and with considering bandgap and specific surface area in the input data, respectively. Reprinted with permission from ref [42]. Copyright 2022, Elsevier.

photocatalytic materials [165].

Not just for crystallised structures, machine learned potentials are useful on amorphous systems as well. Jeong *et al.* comprised total 64 atoms' configurations of Carbon and Nitrogens for AIMD of different densities (2.0, 2.45, 2.95, 3.2, and 3.5 gm cm⁻³) [166]. Using 16 radial and 54 angular components symmetry functions as input features a neural network potential (NNP) for amorphous CN was trained using the SIMPLE-NN package [167]. A comprehensive database for 216 atoms was constructed on a variety of amorphous CN structures, those investigated for spectral fingerprints using DFT approach.

6.2. Catalysis Research

Discovery of CNs and their derivatives are regarded as a revolutionary leap toward artificial catalysis. Catalytic activity involves two half-reactions: (i) Hydrogen Evolution Reaction (HER) at cathode, and, (ii) Oxygen Evolution / Reduction reaction (OER/ORR) at anode. In photocatalysis, photochemical reactions are driven by photons with energies greater than the bandgap. These photons generate electron-hole combination, If they do not recombine, then HER and OER reactions are initiated at the conduction band (CB), and valence band (VB) by electrons and holes, respectively. For that certain conditions have to be satisfied. For example, in case of water splitting the maximum

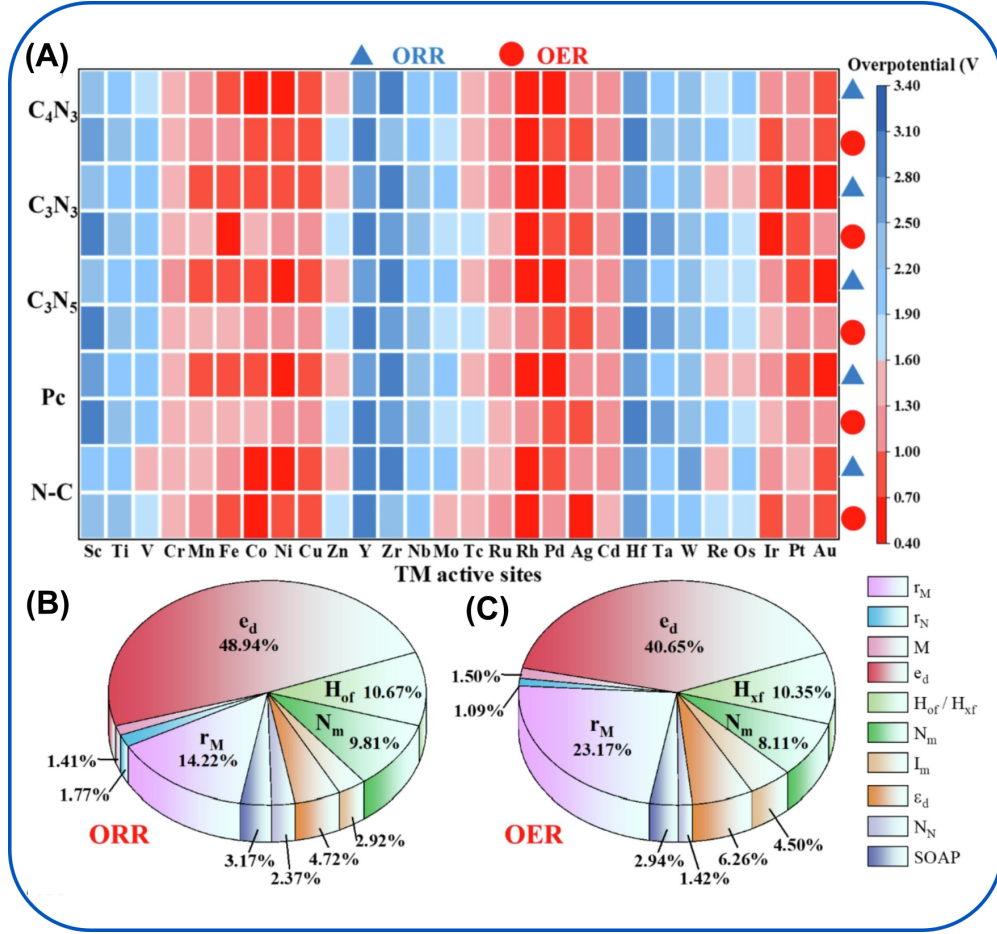
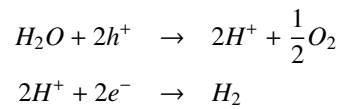


Figure 11: (A) Heat map of ML-predicted ORR/OER overpotentials for SAC@CNs (C₄N₃, C₃N₃, C₃N₅, Pc, N-C). Redder colors indicate higher catalytic activity. Blue triangles represent ORR, red circles represent OER. (B) and (C) Feature importance in RFR models for ORR and OER prediction, respectively. Reprinted with permission from ref [168]. Copyright 2022, Elsevier.

of VB should be more positive than the OER potential ($E_{H_2O/O_2}=1.23, 0.81$ V for pH=0, 7), and the minimum of CB should be more negative than the HER potential ($E_{H^+/H_2}=0, -0.41$ V for pH=0, 7 in normal hydrogen electrode (NHE) scale):



Both of the HER and OER generally are not single step processes. The calculation of Gibbs free energy change for each sub-step is essential for finding the reactional pathway. This can be expressed as

$$\Delta G = \Delta E + \Delta ZPE - T\Delta S + \Delta G_U + \Delta G_{pH}$$

where, ΔE , ΔZPE , ΔS , ΔG_U , and ΔG_{pH} represent the change of adsorption energy, zero-point energy (ZPE),

entropy (S), change of free energy contribution due to electrode potential and ion concentrations, respectively [120]. For HER/OER, ΔE can be computed using DFT through total energy calculations on catalysts with and without adsorbed Hydrogen/Oxygen atom and isolated H_2/O_2 gas molecule as:

$$\Delta E = E_{H+surface} - E_{surface} - \frac{1}{2}E_{H_2/O_2}$$

6.2.1. Hydrogen Evolution Reaction

The Hydrogen Evolution Reaction is a fundamental electrochemical process that involves the reduction of protons (H^+) and electrons (e^-) to produce hydrogen gas. This reaction plays a crucial role in various energy-related technologies, particularly in hydrogen production and fuel cell applications.

Aiming to fabricate single atom catalysts (SACs) from 3d, 4d, and 5d transition metals (TM), metal atoms were set as the active sites on C_6N_3 sheets by Yuan *et al.* [120]. As a primary step, the electronic properties of TM such as atomic number and charge, number of valence electrons, number of d electrons and positions of d band centres, atomic radius, electronegativity in Pauling scale, first ionization energy, electron affinity were considered as features. However, the result was not satisfactory, hence, the distance between TM and N atoms and the atomic charge of the N atom were added as features. Physical parameters of TM showed low linear correlation with the local structure around TM. It demonstrate the importance of feature engineering as preprocessing step.

Similar work using DFT and ML on $SAC@C_3N_4$ was done bu Umer *et al.* [169]. To estimate the model performance, the Monte-Carlo cross validation method was employed. Among the nine distinct ML regression models tested for predicting HER activities, the CatBoost (an extension of GBR) regression model demonstrated the highest accuracy.

Often, a comparison of different models on same data is beneficial. The final model selection is depends on achieving the optimal balance among different factors such as predictive accuracy, computational efficiency, interpretability, and scalability of ML models. They compared different ML regression algorithms including LR, RR, RF regression, feed-forward ANN regression, and finally, found GBR as best performing method to predict HER activity for $TM@C_6N_3$.

Another study on SACs on a different CN, $g-C_3N_4$ was conducted using DFT data by Jyothirmai *et al.* . They identified B, Mn, and Co embedded on $g-C_3N_4$ as highly competent catalysts for hydrogen production from a series of different metals and nonmetals [170]. Comparing different regression models, SVR was found as most effective in this particular study.

In material science most of the dataset are often not as large as needed for effective model building. Hence, multiple datasets or even different types of data have to be integrated to create a comprehensive dataset. A database totalling 767 instances was built from of 106 research articles on experimental $g-C_3N_4$ doped by different elements for photocatalytic hydrogen production by Yan *et al.* [42]. Along with H_2 production criteria, material properties and synthesis conditions were fed to the ML models, and the Hydrogen production rate was derived as output (see,

Figure–10(A–D)). Instead of doing separate feature selection, RF algorithms was adopted for its intrinsic property of rewarding higher weight to important features. Data cleaning is an essential process to ensure data quality and consistency. Eight encoding methods and five scaling techniques were used to scale numerical variables. Also to handle missing values, tree based ML algorithms like XGBoost and CatBoost were selected. Bayesian optimization was adopted for tuning the hyperparameters of ML model. Finally a perfect synthesis condition including the choice of precursor and dopant was extracted.

Besides SACs, heterostructures of CNs with other materials for catalysis steals the show even in ML regime. In a work on a g-C₃N₄/MX₂ heterostructure, another popular scaling method of numerical features “MinMaxScaler” was utilised from the Scikit-Learn library in a hunt for efficient HER [171].

6.2.2. Oxygen Evolution / Reduction reaction

The oxygen evolution reaction and oxygen reduction reaction are fundamental electrochemical processes that involve the exchange of oxygen atoms and electrons at the surface of electrodes. OER refers to the process where oxygen molecules are split into oxygen ions and electrons. ORR, on the other hand, involves the reduction of oxygen molecules by accepting electrons. Both reactions are pivotal in energy conversion and storage technologies, influencing the efficiency and performance of various electrochemical devices.

To validate the feasibility of a single TM embedded in defective g-C₃N₄ for bifunctional oxygen electrocatalysis, a ML model was employed to elucidate the intrinsic correlation between targeted adsorption energy and descriptors [172]. The input dataset included 10 descriptors pertaining to structural and atomic properties. Given the limited size of the dataset, the GBR model was selected as the ML algorithm, which exhibited exceptional performance.

Using DFT, ML, and a cross validation scheme, Wan *et al.* established the best performing ML regression models for ORR/OER [168]. Those models effectively characterized the relationships between readily accessible physical and chemical properties and the overpotentials of C₂N, C₃N, and C₃N₄ related SACs (Figure–11(A–C)). Through this approach, three promising oxygen electrocatalysts were identified with low overpotentials.

In catalytic research stability of the material is a prime concern. The experimental data for stability comes in a time domain data form. To forecast the stability of prepared samples, data from chronoamperometric measurement for 800 s was taken [173]. Long and short term memory (LSTM) technique of recurrent neural network was utilised. The model forecasted a nominal 0.12% decrease in stability of photo-anodes for an extended period.

6.3. Environmental Remedy

Graphitic CN has established itself as a versatile material with wide-ranging applications in environmental remediation and sustainable technology. Its two-dimensional structure, enriched with nitrogen, enables efficient photocatalytic activity under visible light, making it effective in degrading organic pollutants and oxidizing harmful gases in both water and air. This capability finds practical use in wastewater treatment, air purification systems, and industrial emissions control, where g-C₃N₄'s ability to be tailored for enhanced adsorption further enhances its utility.

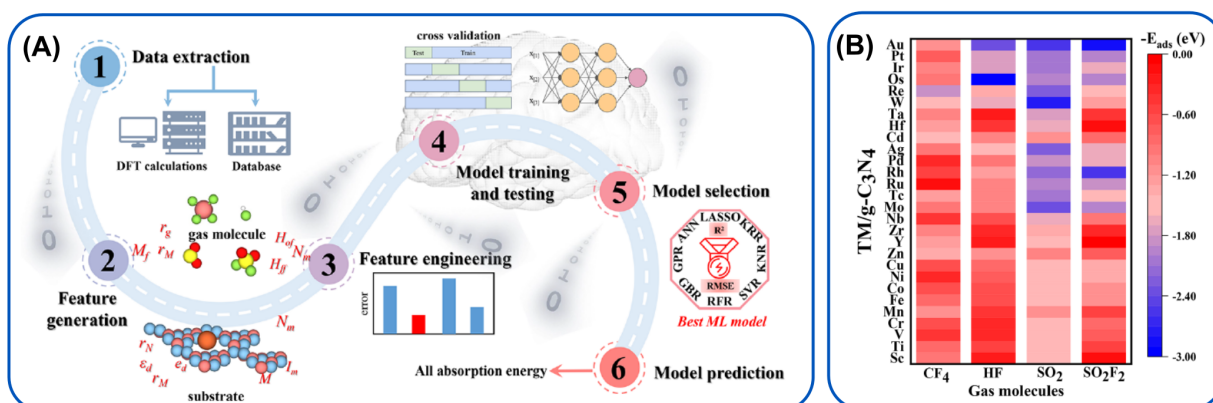


Figure 12: (A) Machine learning workflow for exploring interaction strengths among four decomposed CF_3SO_2F gas products and 28 TM/ $g-C_3N_4$ combinations, employing common ML algorithms. (B) Absorption energies calculated for interactions between 28 distinct types of TM supported on $g-C_3N_4$ and four different decomposition gases. Reprinted with permission from ref [174]. Copyright 2023, American Chemical Society.

One of its successful application is found in CO_2 reduction reaction (CO_2RR). The CO_2RR involves the electrochemical reduction of carbon dioxide (CO_2) to produce valuable chemicals or fuels. It typically occurs in an electrolytic cell where CO_2 is supplied to the cathode, and a voltage is applied to drive the reduction process. Beside carbon monoxide (CO), CO_2RR can also produce other products such as methane (CH_4), ethylene (C_2H_4), formic acid ($HCOOH$), and even higher hydrocarbons, depending on the catalyst and operating conditions used. CO_2RR research aims to improve the efficiency and selectivity of these reactions to make them commercially viable for carbon capture and utilization, as well as for renewable energy storage applications.

Zhu *et al.* used DFT and ML together to predict free energy change in the reactional pathway for reduction of CO_2 by metal-oxide-frameworks (MOF), metal-zeolites, metal-doped 2D materials including graphene, and $g-C_3N_4$ [175]. The descriptors include the reaction pathways, the metal involved, the charge transfer (CT) occurring between the metal and reaction intermediate, the hydrogen bond interaction between the intermediate and the zeolite framework, and the geometric configuration. A variety of ML algorithms were tested including GBR, MLR, XGBoost, SVR, LASSO, Extra-Trees, KNN, Decision tree, LR, and least absolute shrinkage, ANNs. A total of 34 catalysts were tested and predicted the final products in CO_2RR and with 91% accuracy. XGBoost, ExtraTrees, and GBR performed best.

Goliaei evaluated cobalt single atoms and Co_2O_2 clusters supported on $g-C_3N_4$ as catalysts for CO_2RR [176]. Linear regression, neural-network based, and ensemble tree model combined with GBR were considered. After training these models on a designated training set, they assessed their performance by comparing RMSE on a test set. The ensemble tree model which was proved to be useful for the studies on energy materials, exhibited superior performance, highlighting its effectiveness for small datasets in this application. Employment of ML in CO_2RR by CNs well-documented across various studies [177].

The study by Zhao *et al.* investigated the efficacy of single metal atom catalysts embedded on g-C₃N₄ for formic acid dehydrogenation, focusing on their impact on the adsorption energy of formic acid. According to the results from ML models, the adsorption strength of formic acid on M@g-C₃N₄ is predominantly influenced by two critical features: the higher electronegativity of the metal atom and the more negative d-band centre of the metal atom. The ML scheme utilized several widely adopted models, including RR, RFR, ANN, and GBR, implemented through the scikit-learn package. These models were employed to analyse and predict data patterns, leveraging their respective strengths in regression tasks to achieve robust and accurate predictions within the study's framework.

Chen *et al.* targeted nitrogen reduction reaction (NRR) by TM single atom photocatalysts embedded on C₃N₄ from theoretical data [178]. Expressing $\Delta G_U = eU$, where, U is the applied electrode potential, they set the onset potential U as the target property. They considered both of electronic and geometric properties as features, totalling 8 in number. Sure Independence Screening and Sparsity Optimization (SISSO) is a ML method curated for materials science applications [179]. It aims to identify as well as optimize the most relevant descriptors while maintaining interpretability side-by-side. Using backward elimination method and SISSO, they identified three descriptors correlating with the target property. Finally Ru was predicted as a promising candidate single photocatalyst residing on g-C₃N₄ for NRR. Tungsten atoms supported on g-C₃N₄ was identified as promising SACs for the NRR, characterized by low limiting-potential and high selectivity towards ammonia, as predicted by ML models by Zhang *et al.* [180]. Similar study on NRR by TM embedded C₆N₆ was conducted by Mukherjee *et al.* [181].

Li *et al.* employed RF, XGBoost and GBR models to predict the photocatalytic purification rate of NO on g-C₃N₄ based catalysts using 255 data points with 14 input features [182]. They employed Shapley additive explanation, feature importance analysis, and partial dependence plots to investigate the influence of input features on the target variable, the NO removal rate.

Miodyńska *et al.* take the advantage of ML for selecting optimal Cs₃Bi₂X₉ stoichiometry with various amounts of X = Cl, Br, and I halides and their combinations on C₃N₄ matrix for degradation of pollutants under visible light [183]. PCA was used for virtual screening of a plethora of binary structures. Based on the structural similarity grouping of the Cs₃Bi₂X₉ perovskites were done and a possible relationship was determined between these structures and their photocatalytic performance. In a separate investigation, ANN based ML modeling was utilised to estimate the photodegradation efficiency of g-C₃N₄ for the degradation of the organic pollutant Reactive Black 5 [184].

Antibiotic pollution in water is another growing environmental concern due to the widespread use of antibiotics in healthcare, agriculture, and veterinary practices. Once in aquatic environments, antibiotics can persist and accumulate, posing risks to aquatic organisms and potentially entering the food chain. Gordanshekan *et al.* synthesised Bi₂WO₆/g-C₃N₄ and Bi₂WO₆/TiO₂ heterojunctions for adsorption/degradation of Cefixime antibiotic in aqueous environment [185]. ML scheme involving ANNs with 18 hidden neurons performed best for predicting of the kinetics of the photocatalytic reaction. In another study on g-C₃N₄/Ce-ZnO/Ti, the Cefixime degradation was taken as the targeted output for ANN and the input parameters were number of electrode, pH, power of visible light, electrolyte concentration, pollutant concentration [186]. Eight ML methods were employed to predict the performance

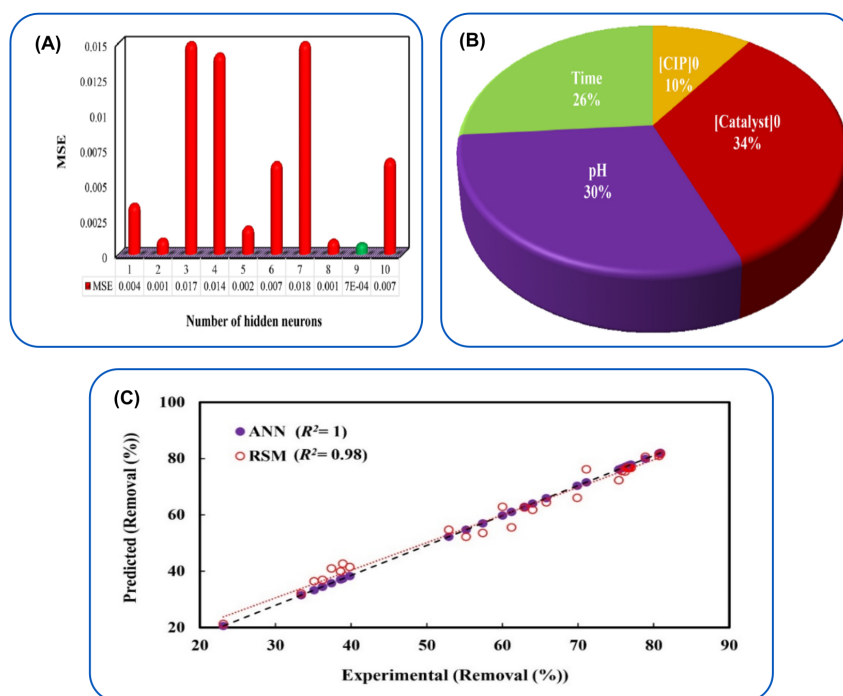


Figure 13: (A) Mean squared error (MSE) of designed networks plotted against the number of hidden neurons. (B) Relative importance of operational parameters on the efficiency of CIP (Ciprofloxacin) removal. (C) Comparison between experimental results and predictions obtained using Response Surface Methodology coupled with ANN. Reprinted with permission from ref [187] Copyright 2023 Elsevier.

of g-C₃N₄ based photocatalysts in degrading tetracycline [188]. Starting from 431 experimentally obtained records from literature, the XGBoost model utilized an optimized leaves parallel processing strategy to effectively capture the experimental parameters of tetracycline photodegradation. This approach mirrors the reaction generation process involved in tetracycline degradation facilitated by g-C₃N₄ based photocatalysts.

Multivariate ANNs were used for predicting the Ciprofloxacin degradation efficiency of ZnO/g-C₃N₄ by Gupta *et al.* [189]. Another study investigated the efficiency of a quaternary composite and assessed the relative importance of operational parameters using ANN [187]. The importance of operational environments as features and the performance of ANN is presented in Figure–13. The photocatalytic degradation efficiency of tetracycline hydrochloride by Fe₃O₄/g-C₃N₄/rGO predicted using ANN hybridised with Particle Swarm Optimization (PSO) model was found to be at par with experimental results by Shan *et al.* [190].

Not only the removal of pollutant, environmental research also aims the production of pollution free energy sources, like green hydrogen production, synthesis of biodiesel, enhancing the performance of solar cells, etc. Taib's research focused on transesterification of algal oil for biodiesel production, aiming to advance pollution-free energy sources [191]. The study utilized ANN and GRNN for modeling and optimizing the transesterification process. The methanol to oil ratio is identified as a critical factor influencing the yield of the blend in transesterification reactions.

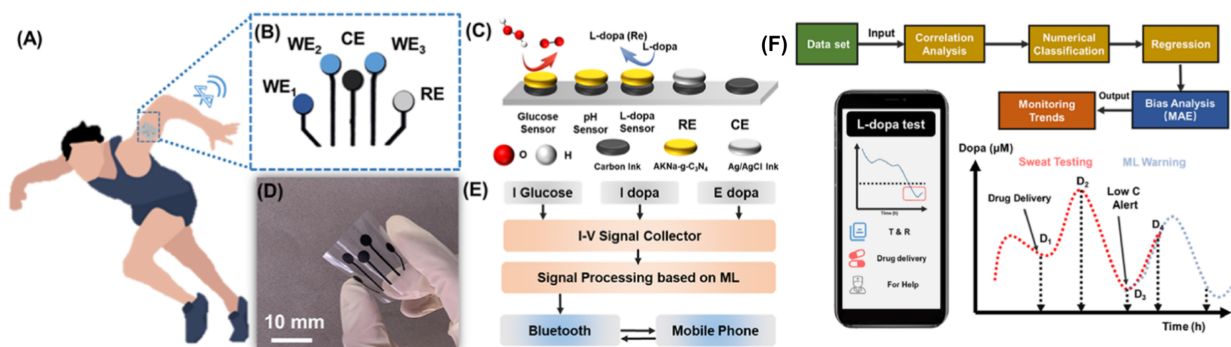


Figure 14: A comprehensive workflow of wireless sweat sensing devices combining (A) Schematic diagram for real-time monitoring, (B) primary structural components within the sensing chip, (C) A model illustrating the operational mechanism of electrode, (D) Photographic depiction of an unencapsulated sensing chip, (E) Logical diagram delineating the operational sequence of the wireless transmission module, focusing on signal acquisition, transduction, and data output from three distinct sensors and, (F) Schematic diagram illustrating the processing model for simulated human drug delivery based on ANN. Reprinted with permission from ref [192] Copyright 2022 American Chemical Society.

A recent study involved the adsorption of gases produced by decomposition of CF_3SO_2 (e.g., SO_2 , SO_2F_2 , and CF_4) on $\text{TM@g-C}_3\text{N}_4$ as presented in Figure–12. The focus was on predicting adsorption energies with high accuracy using an ML approach. A comprehensive process involving feature engineering, data extraction, and model training was undertaken with Scikit-learn and PyTorch packages. Eight supervised ML algorithms were employed: GBR, RF, SVR, KNR, KRR, LASSO, ANN, and GPR. Among these, the SVR model demonstrated superior performance on both training and test sets, achieving a lower $\text{RMSE} = 0.223 \text{ eV}$ and a higher score of $R^2 = 0.911$, indicating its effectiveness [174].

6.4. Bio-medical application

Material science plays a pivotal role in medical diagnostic technologies through enabling the evolution of advanced materials that improve sensitivity, and reliability in identification tools. Across diverse fields such as biosensors, diagnostic imaging, lab-on-a-chip devices, and nanomedicine, material scientists are leaving their footprints.

Dopamine, a key neurotransmitter in humans and mammals, regulates central nervous system functions including behaviour, learning, and memory. Dysregulation of dopamine levels is linked to neurological disorders like Parkinson's disease, schizophrenia, and Tourette syndrome, underscoring the critical need for accurate and sensitive dopamine detection in clinical diagnosis. Electrochemiluminescence (ECL) is an effective tool for dopamine detection and C_3N_4 derived materials are promising agent for ECL detection. Li *et al.* carried out multiparameter concentration prediction of dopamine using DNN assisted technique on $\text{Ag@g-C}_3\text{N}_4$ [193]. Each of the eight dopamine concentrations underwent five measurements, resulting in a data matrix of 16 parameters across 8 concentrations and 5 parallel tests, which was then analyzed using the DNN algorithm. There was a strong correlation between experimental and ML predicted dopamine concentrations across the range from 0.1 nM to 1 mM, demonstrating the accurate prediction capability of the multicolour ECL detection array in conjunction with the DNN algorithm. The DNN-assisted model

achieves a high $R^2 = 0.99861$ and $RMS E = 0.0997$ value, indicating excellent predictive accuracy for dopamine concentration.

In Parkinson's disease treatment, monitoring L dopa levels in sweat offers insights into pharmacological management and non-motor complications. Nanozymes, like layered g-C₃N₄ are promising due to their robust catalytic activity, stability, and customizable performance, potentially replacing natural enzymes [194, 195]. Customized dose criteria based on long term serial assessments of L dopa levels in sweat could optimize patient treatment. Utilising raw electrical signals of sweat analytes, along with factors like time, pH, and daily activity, as training data for ML models, enabled real time prediction of L-dopa levels (Figure-14) in a recent study by Yu *et al.* [192]. This approach supported more effective pharmacological management of Parkinson's disease patients. Various ML algorithms including LR, MLRs, CNNs, and ANNs were employed to predict trends in L-dopa levels in sweat post individual dosing. These models also provided estimations for the optimal timing of next doses based on insights gained from the dataset.

In a significant work, Au@g-C₃N₄/ZnO was synthesized using a straightforward chemical technique to advance the development of triboelectric nanogenerators (TENG) for achieving high accuracy in biomechanical motion recognition [196]. The outputs from ZnAuCN based TENG sensors were analysed using supervised ML. Notably, no significant performance improvement was observed with alternative algorithms such as ANN or SVM.

7. Future Perspective of ML Research in GAI Regime

CNs are regarded as future materials with prospects in advanced application in versatile fields like photocatalysis, energy storage, and electronic devices. The integration of ML in the research of CN materials holds immense potential to revolutionize the field. ML-driven approaches significantly advance the development and application of CNs as discussed in the previous sections by accelerating discovery, optimizing synthesis, predicting properties, and enabling sustainable practices.

Generative AI is the next paradigm shift in the field of automation. In its early stages, it is showing promise in material science. The Deep Inorganic Material Generator (DING) proposed by Pathak *et al.* uses conditional VARs (CVAEs) and a predictor module consisting of three DNNs trained to predict the formation enthalpy, the volume per atom and the energy per atom to discover new materials [197]. Using materials from the ICSD database as training data, a GAN-based ML model, MatGAN for the efficient generation of new hypothetical inorganic materials [198]. Using this Song *et al.* discovered 267,489 new potential 2D material compositions, with 1,485 highly probable compositions, predicted 101 crystal structures, and confirmed 92 2D/layered materials via DFT formation energy calculations [199].

Court *et al.* propose an autoencoder-based generative deep representation learning pipeline for optimizing 3D crystal structures and predicting eight target properties: formation energy per atom, energy per atom, bulk modulus, shear modulus, refractive index, dielectric constant, Poisson ratio, and bandgap [200]. Based on data from the Mate-

rials Project, the pipeline generated novel binary alloys, ternary perovskites, and Heusler compounds using VAE and predicted the properties using a GNN. A plethora of recent generative AI approaches for automated material discovery have focused on various applications, including drug discovery, solar cells, and battery materials, ranging from novel molecules to complex crystal structures [201, 202, 203, 204, 205]. Some recent review articles have compiled various works in this field [206, 207].

Not only limited to material discovery, but GAI models have also been employed for the autonomous determination of phase diagrams with minimal human supervision [208].

In catalysis research, GAI is gaining popularity. The GAN based approach, called Catalysis Clustering, incorporates domain knowledge into the clustering process by generating catalysts—special synthetic points drawn from the original data distribution. These catalysts are verified to improve clustering quality based on a domain-specific metric [209]. DFT was combined with a GAN to artificially propose heterogeneous catalysts using a DFT calculated dataset. This approach was demonstrated on the NH_3 formation reaction on Rh–Ru alloy surfaces [210]. Conditional GAN predicted transition state (TS) geometries by mapping reactants and products directly to the TS space. This method generated TS guesses from Cartesian coordinates alone, bypassing costly reaction path mapping and aiming for simplicity, general applicability, and easy expansion [211].

GAI is targeted to make the coding or research job easier in every sense. The Generative Toolkit for Scientific Discovery (GT4SD) is an open-source library for training and using state-of-the-art generative models in organic material design. It supports execution, training, fine-tuning, and deployment via Python or CLI, with pre-trained models also accessible through web apps [212].

Our discussion clearly indicates that research on CN-based materials is undergoing a significant paradigm shift. Traditional experimental and computational investigations are now increasingly complemented by ML methods. These methods are proving promising in discovering new CN-supported SACs, CN based heterostructures, and pathways for HER, OER/ORR, and pollutant removal reactions.

Although the application of state-of-the-art generative modeling to CNs has not yet been reported, future ML research is expected to focus on advanced material discovery using generative models, such as GANs and VAEs, to predict novel structures with tailored properties. This research will optimize synthesis pathways and experimental parameters to achieve higher purity and yield, and predict critical properties, including electronic, mechanical, and thermal characteristics. Efforts will also include data augmentation to enhance model training and inverse design to work backward from desired properties to potential structures. Integrating ML with traditional research methods will drive innovation in CN materials, contributing to energy, environmental, and technological advancements for the betterment of society.

Declaration of competing interest. The authors declare that they have no known competing financial interests or personal relationships that could have appeared to influence the work reported in this paper.

CRedit authorship contribution statement. **DM:** Conceptualisation, Editing, Writing original draft. **SD:** Conceptualisation, Editing, Supervision, Writing original draft. **DJ:** Conceptualization, Editing, Supervision, Finalizing Manuscript.

Acknowledgements

DM would like to thank the Council of Scientific and Industrial Research (CSIR), India for providing financial support as Senior Research Fellow.

References

- [1] K. S. Novoselov, A. K. Geim, S. V. Morozov, D.-e. Jiang, Y. Zhang, S. V. Dubonos, I. V. Grigorieva, A. A. Firsov, Electric field effect in atomically thin carbon films, *science* 306 (5696) (2004) 666–669.
- [2] Z. Zhao, Y. Sun, F. Dong, Graphitic carbon nitride based nanocomposites: a review, *Nanoscale* 7 (1) (2015) 15–37.
- [3] A. Wang, X. Zhang, M. Zhao, Topological insulator states in a honeycomb lattice of s-triazines, *Nanoscale* 6 (19) (2014) 11157–11162.
- [4] S. Datta, P. Singh, D. Jana, C. B. Chaudhuri, M. K. Harbola, D. D. Johnson, A. Mookerjee, Exploring the role of electronic structure on photo-catalytic behavior of carbon-nitride polymorphs, *Carbon* 168 (2020) 125–134.
- [5] R. Tan, Z. Li, P. Zhou, Z. Zou, W. Li, L. Sun, Dirac semimetals in homogeneous holey carbon nitride monolayers, *The Journal of Physical Chemistry C* 125 (11) (2021) 6082–6089.
- [6] S. Jana, D. Mondal, R. Roy, S. Kanungo, D. Jana, Spontaneous dumbbell formations via surface functionalization of the c_3n monolayer with versatile electronic and mechanical properties, *The Journal of Physical Chemistry C* 127 (36) (2023) 18001–18014.
- [7] Y. Zhao, Z. Dai, C. Lian, S. Meng, Exotic thermoelectric behavior in nitrogenated holey graphene, *RSC advances* 7 (42) (2017) 25803–25810.
- [8] N. Rono, J. K. Kibet, B. S. Martincigh, V. O. Nyamori, A review of the current status of graphitic carbon nitride, *Critical Reviews in Solid State and Materials Sciences* 46 (3) (2021) 189–217.
- [9] Y. Dong, Q. Wang, H. Wu, Y. Chen, C.-H. Lu, Y. Chi, H.-H. Yang, Graphitic carbon nitride materials: sensing, imaging and therapy, *Small* 12 (39) (2016) 5376–5393.
- [10] J. Liu, H. Wang, M. Antonietti, Graphitic carbon nitride “reloaded”: emerging applications beyond (photo) catalysis, *Chemical Society Reviews* 45 (8) (2016) 2308–2326.
- [11] T. Miller, A. B. Jorge, T. Suter, A. Sella, F. Corà, P. McMillan, Carbon nitrides: synthesis and characterization of a new class of functional materials, *Physical Chemistry Chemical Physics* 19 (24) (2017) 15613–15638.
- [12] H. Wang, X. Zhang, Y. Xie, Recent progress in ultrathin two-dimensional semiconductors for photocatalysis, *Materials Science and Engineering: R: Reports* 130 (2018) 1–39.
- [13] X. Kong, X. Liu, Y. Zheng, P. K. Chu, Y. Zhang, S. Wu, Graphitic carbon nitride-based materials for photocatalytic antibacterial application, *Materials Science and Engineering: R: Reports* 145 (2021) 100610.
- [14] Y. Chen, B. Zhang, Y. Liu, J. Chen, H. Pan, W. Sun, Graphitic carbon nitride-based electrocatalysts for energy applications, *Materials Today Catalysis* (2023) 100003.
- [15] S. Thomas, S. Anas, J. Joy, *Synthesis, Characterization, and Applications of Graphitic Carbon Nitride: An Emerging Carbonaceous Material*, Elsevier, 2022.
- [16] J. Mahmood, E. K. Lee, M. Jung, D. Shin, H.-J. Choi, J.-M. Seo, S.-M. Jung, D. Kim, F. Li, M. S. Lah, et al., Two-dimensional polyaniline (c_3n) from carbonized organic single crystals in solid state, *Proceedings of the National Academy of Sciences* 113 (27) (2016) 7414–7419.
- [17] S. Yang, W. Li, C. Ye, G. Wang, H. Tian, C. Zhu, P. He, G. Ding, X. Xie, Y. Liu, et al., C_3n —a 2d crystalline, hole-free, tunable-narrow-bandgap semiconductor with ferromagnetic properties, *Advanced Materials* 29 (16) (2017) 1605625.

- [18] M. Bonacci, M. Zanfognini, E. Molinari, A. Ruini, M. J. Caldas, A. Ferretti, D. Varsano, Excitonic effects in graphene-like c_3n , *Physical Review Materials* 6 (3) (2022) 034009.
- [19] W. Jiao, R. Hu, S. Han, Y. Luo, H. Yuan, M. Li, H. Liu, Surprisingly good thermoelectric performance of monolayer c_3n , *Nanotechnology* 33 (4) (2021) 045401.
- [20] A. Bafekry, S. Farjami Shayesteh, F. M. Peeters, C_3n monolayer: Exploring the emerging of novel electronic and magnetic properties with adatom adsorption, functionalizations, electric field, charging, and strain, *The Journal of Physical Chemistry C* 123 (19) (2019) 12485–12499.
- [21] Y. Yong, H. Cui, Q. Zhou, X. Su, Y. Kuang, X. Li, C_2n monolayer as nh_3 and no sensors: A dft study, *Applied Surface Science* 487 (2019) 488–495.
- [22] P. Gao, L. Zhang, C. Fu, Y. Tian, X. Li, X. Li, J. Yang, Promoting water activation by photogenerated holes in monolayer c_2n , *The Journal of Physical Chemistry Letters* 13 (15) (2022) 3332–3337.
- [23] L. Li, J. Li, Y. Yu, Y. Song, J. Li, X. Liu, F. M. Peeters, X. Chen, G. Liu, Rectangular carbon nitrides c_4n monolayers with a zigzag buckled structure: Quasi-one-dimensional dirac nodal lines and topological flat edge states, *arXiv preprint arXiv:2401.03402* (2024).
- [24] S. Tang, Z. Yang, W. Liu, C. Liu, S. Bai, J. Zhang, D. Luo, Exploring the anchoring mechanism of polyselenides on c_4n_3 monolayer as selenium host material: A first-principles study, *Diamond and Related Materials* 138 (2023) 110263.
- [25] C. He, Y. Liao, T. Ouyang, H. Zhang, H. Xiang, J. Zhong, Flat-band based high-temperature ferromagnetic semiconducting state in the graphitic c_4n_3 monolayer, *Fundamental Research* (2023).
- [26] N. Zhang, Z.-G. Fu, X. Wang, X.-P. Fu, Y. Hong, Y.-T. Shi, P. Zhang, First-principles prediction of mg decoration on monolayer $g-c_6n_7$ as a promising a hydrogen storage media, *International Journal of Hydrogen Energy* 50 (2024) 136–147.
- [27] R. Zhang, Z. Wang, Q. Hou, X. Yuan, Y. Yong, H. Cui, X. Li, First-principles insights into the c_6n_7 monolayer as a highly efficient sensor and scavenger for the detection of selective volatile organic compounds, *RSC advances* 13 (41) (2023) 28703–28712.
- [28] F. Dong, Y. Li, Z. Wang, W.-K. Ho, Enhanced visible light photocatalytic activity and oxidation ability of porous graphene-like $g-c_3n_4$ nanosheets via thermal exfoliation, *Applied Surface Science* 358 (2015) 393–403.
- [29] F. Wu, Y. Liu, G. Yu, D. Shen, Y. Wang, E. Kan, Visible-light-absorption in graphitic c_3n_4 bilayer: enhanced by interlayer coupling, *The Journal of Physical Chemistry Letters* 3 (22) (2012) 3330–3334.
- [30] W. Wei, S. Yang, G. Wang, T. Zhang, W. Pan, Z. Cai, Y. Yang, L. Zheng, P. He, L. Wang, et al., Bandgap engineering of two-dimensional c_3n bilayers, *Nature Electronics* 4 (7) (2021) 486–494.
- [31] W. Xu, C. Chen, C. Tang, Y. Li, L. Xu, Design of boron doped c_2n - c_3n coplanar conjugated heterostructure for efficient her electrocatalysis, *Scientific Reports* 8 (1) (2018) 5661.
- [32] D. Liang, T. Jing, Y. Ma, J. Hao, G. Sun, M. Deng, Photocatalytic properties of $g-c_6n_6/g-c_3n_4$ heterostructure: a theoretical study, *The Journal of Physical Chemistry C* 120 (42) (2016) 24023–24029.
- [33] X. Yuan, Y. Yong, Q. Hou, W. Guo, H. Cui, X. Li, X. Li, The design of cn/c_3n_2 heterostructures and the potential as gas sensor and scavenger for sf_6 decomposed gases, *Surfaces and Interfaces* (2024) 104532.
- [34] M. Fawaz, R. Bahadur, N. P. Dharmarajan, J.-H. Yang, C. Sathish, A. M. Sadanandan, V. Perumalsamy, G. Singh, X. Guan, P. Kumar, et al., Emerging trends of carbon nitrides and their hybrids for photo-/electro-chemical energy applications, *Carbon* 214 (2023) 118345.
- [35] P. Roy, A. Pramanik, P. Sarkar, Graphitic carbon nitride sheet supported single-atom metal-free photocatalyst for oxygen reduction reaction: A first-principles analysis, *The Journal of Physical Chemistry Letters* 12 (11) (2021) 2788–2795.
- [36] D. Adekoya, S. Zhang, M. Hankel, Boosting reversible lithium storage in two-dimensional c_3n_4 by achieving suitable adsorption energy via si doping, *Carbon* 176 (2021) 480–487.
- [37] Z. Liu, X. Fu, M. Li, F. Wang, Q. Wang, G. Kang, F. Peng, Novel silicon-doped, silicon and nitrogen-codoped carbon nanomaterials with high activity for the oxygen reduction reaction in alkaline medium, *Journal of Materials Chemistry A* 3 (7) (2015) 3289–3293.
- [38] S. Kaur, J. Singh, A. Kumar, S. Srivastava, K. Tankeshwar, Energetics and electronic structure of novel hybrid dumbbell monolayers, in: *AIP Conference Proceedings*, Vol. 2115, AIP Publishing, 2019.

- [39] X. Duan, B. Zhou, X. Wang, Diverse electronic structures governed by n-substitution in stable two-dimensional dumbbell carbonitrides, *Applied Surface Science* 609 (2023) 155463.
- [40] D. Morgan, R. Jacobs, Opportunities and challenges for machine learning in materials science, *Annual Review of Materials Research* 50 (2020) 71–103.
- [41] J. R. Kitchin, Machine learning in catalysis, *Nature Catalysis* 1 (4) (2018) 230–232.
- [42] L. Yan, S. Zhong, T. Igou, H. Gao, J. Li, Y. Chen, Development of machine learning models to enhance element-doped g-c₃n₄ photocatalyst for hydrogen production through splitting water, *International Journal of Hydrogen Energy* 47 (80) (2022) 34075–34089.
- [43] H. Mai, T. C. Le, D. Chen, D. A. Winkler, R. A. Caruso, Machine learning for electrocatalyst and photocatalyst design and discovery, *Chemical Reviews* 122 (16) (2022) 13478–13515.
- [44] E. Shahini, N. Chaulagain, K. Shankar, T. Tang, Predicting free energies of exfoliation and solvation for graphitic carbon nitrides using machine learning, *ACS Applied Materials & Interfaces* 15 (46) (2023) 53786–53801.
- [45] T. O. Owolabi, M. A. Abd Rahman, Prediction of band gap energy of doped graphitic carbon nitride using genetic algorithm-based support vector regression and extreme learning machine, *Symmetry* 13 (3) (2021) 411.
- [46] J. Li, C. Cao, J. Hao, H. Qiu, Y. Xu, H. Zhu, Self-assembled one-dimensional carbon nitride architectures, *Diamond and related materials* 15 (10) (2006) 1593–1600.
- [47] G. P. Mane, D. S. Dhawale, C. Anand, K. Ariga, Q. Ji, M. A. Wahab, T. Mori, A. Vinu, Selective sensing performance of mesoporous carbon nitride with a highly ordered porous structure prepared from 3-amino-1, 2, 4-triazine, *Journal of materials chemistry A* 1 (8) (2013) 2913–2920.
- [48] K. Srinivasu, B. Modak, S. K. Ghosh, Porous graphitic carbon nitride: a possible metal-free photocatalyst for water splitting, *The Journal of Physical Chemistry C* 118 (46) (2014) 26479–26484.
- [49] Y. Wang, L. Liu, T. Ma, Y. Zhang, H. Huang, 2d graphitic carbon nitride for energy conversion and storage, *Advanced Functional Materials* 31 (34) (2021) 2102540.
- [50] S. Kumar, V. R. Battula, K. Kailasam, Single molecular precursors for cxny materials-blending of carbon and nitrogen beyond g-c₃n₄, *Carbon* 183 (2021) 332–354.
- [51] X. Chen, J.-w. Li, X. Dou, P. Gao, Computational evaluation of mg-decorated g-cn as clean energy gas storage media, *International Journal of Hydrogen Energy* 46 (71) (2021) 35130–35136.
- [52] Z. Chu, X. Kang, X. Duan, Single metal atom anchored on a cn monolayer as an excellent electrocatalyst for the nitrogen reduction reaction, *Physical Chemistry Chemical Physics* 23 (4) (2021) 2658–2662.
- [53] B. Ram, H. Mizuseki, Tetrahexcarbon: A two-dimensional allotrope of carbon, *Carbon* 137 (2018) 266–273.
- [54] Q. Wei, Y. Yang, A. Gavrilov, X. Peng, A new 2d auxetic cn₂ nanostructure with high energy density and mechanical strength, *Physical Chemistry Chemical Physics* 23 (7) (2021) 4353–4364.
- [55] S. Zhang, J. Zhou, Q. Wang, P. Jena, Beyond graphitic carbon nitride: nitrogen-rich penta-cn₂ sheet, *The Journal of Physical Chemistry C* 120 (7) (2016) 3993–3998.
- [56] S. Zhang, J. Zhou, Q. Wang, X. Chen, Y. Kawazoe, P. Jena, Penta-graphene: A new carbon allotrope, *Proceedings of the National Academy of Sciences* 112 (8) (2015) 2372–2377.
- [57] F. Li, K. Tu, H. Zhang, Z. Chen, Flexible structural and electronic properties of a pentagonal b 2 c monolayer via external strain: a computational investigation, *Physical Chemistry Chemical Physics* 17 (37) (2015) 24151–24156.
- [58] A. Lopez-Bezanilla, P. B. Littlewood, σ – π -band inversion in a novel two-dimensional material, *The Journal of Physical Chemistry C* 119 (33) (2015) 19469–19474.
- [59] J. Mahmood, E. K. Lee, M. Jung, D. Shin, I.-Y. Jeon, S.-M. Jung, H.-J. Choi, J.-M. Seo, S.-Y. Bae, S.-D. Sohn, et al., Nitrogenated holey two-dimensional structures, *Nature communications* 6 (1) (2015) 6486.
- [60] Z. Tian, N. López-Salas, C. Liu, T. Liu, M. Antonietti, C₂n: A class of covalent frameworks with unique properties, *Advanced Science* 7 (24) (2020) 2001767.

- [61] L. Wang, X. Zheng, L. Chen, Y. Xiong, H. Xu, Van der waals heterostructures comprised of ultrathin polymer nanosheets for efficient z-scheme overall water splitting, *Angewandte Chemie International Edition* 57 (13) (2018) 3454–3458.
- [62] Y. Z. Abdullahi, T. L. Yoon, T. L. Lim, Elastic and electronic properties of c₂n monolayer: first-principles calculation, *Materials Research Express* 6 (2) (2018) 025601.
- [63] Z. Xue, R. Tan, H. Wang, J. Tian, X. Wei, H. Hou, Y. Zhao, A novel tetragonal t-c₂n supported transition metal atoms as superior bifunctional catalysts for oer/orr: From coordination environment to rational design, *Journal of Colloid and Interface Science* 651 (2023) 149–158.
- [64] Y. Wang, Y. Ding, Stable puckered c₂n₂ nanosheet with giant anisotropic hole carrier mobility: insights from first-principles, *Journal of Materials Chemistry C* 8 (44) (2020) 15655–15663.
- [65] L.-B. Shi, S. Cao, J. Zhang, X.-M. Xiu, H.-K. Dong, Mechanical behaviors and electronic characteristics on two-dimensional c₂n₃ and c₂n₃h: First principles calculations, *Physica E: Low-dimensional Systems and Nanostructures* 103 (2018) 252–263.
- [66] T. S. Miller, T. M. Suter, A. M. Telford, L. Picco, O. D. Payton, F. Russell-Pavier, P. L. Cullen, A. Sella, M. S. Shaffer, J. Nelson, et al., Single crystal, luminescent carbon nitride nanosheets formed by spontaneous dissolution, *Nano letters* 17 (10) (2017) 5891–5896.
- [67] J.-Q. Zhou, L. Li, C. Fu, J. Wang, P. Fu, C.-P. Kong, F.-Q. Bai, R. I. Eglitis, H.-X. Zhang, R. Jia, A novel tc₃n and seawater desalination, *Nanoscale* 12 (8) (2020) 5055–5066.
- [68] X. Cai, J. Chen, H. Wang, Y. Ni, Y. Chen, R. B. King, C₃n₂: the missing part of highly stable porous graphitic carbon nitride semiconductors, *Nanoscale Horizons* 8 (5) (2023) 662–673.
- [69] X. Wang, K. Maeda, A. Thomas, K. Takanabe, G. Xin, J. M. Carlsson, K. Domen, M. Antonietti, A metal-free polymeric photocatalyst for hydrogen production from water under visible light, *Nature Materials* 8 (1) (2009) 76–80.
- [70] Y. Luo, Y. Yan, S. Zheng, H. Xue, H. Pang, Graphitic carbon nitride based materials for electrochemical energy storage, *Journal of materials chemistry A* 7 (3) (2019) 901–924.
- [71] A. Ghosh, S. Mandal, P. Sarkar, 2d homogeneous holey carbon nitride: An efficient anode material for li-ion batteries with ultrahigh capacity, *ChemPhysChem* 23 (15) (2022) e202200182.
- [72] H. Pan, Graphitic carbon nitride nanotubes as li-ion battery materials: a first-principles study, *The Journal of Physical Chemistry C* 118 (18) (2014) 9318–9323.
- [73] J. Chen, Z. Mao, L. Zhang, D. Wang, R. Xu, L. Bie, B. D. Fahlman, Nitrogen-deficient graphitic carbon nitride with enhanced performance for lithium ion battery anodes, *ACS nano* 11 (12) (2017) 12650–12657.
- [74] Y. Wang, X. Wang, M. Antonietti, Y. Zhang, Facile one-pot synthesis of nanoporous carbon nitride solids by using soft templates, *ChemSusChem: Chemistry & Sustainability Energy & Materials* 3 (4) (2010) 435–439.
- [75] P. Praus, L. Svoboda, M. Ritz, I. Troppová, M. Šihor, K. Kočí, Graphitic carbon nitride: Synthesis, characterization and photocatalytic decomposition of nitrous oxide, *Materials Chemistry and Physics* 193 (2017) 438–446.
- [76] H. Piao, G. Choi, X. Jin, S.-J. Hwang, Y. J. Song, S.-P. Cho, J.-H. Choy, Monolayer graphitic carbon nitride as metal-free catalyst with enhanced performance in photo-and electro-catalysis, *Nano-micro letters* 14 (1) (2022) 55.
- [77] C. Moreira Da Silva, M. Vallet, C. Semion, T. Blin, R. Saint-Martin, J. Leroy, D. Dragoë, F. Brisset, C. Gillet, R. Guillot, et al., A simple and efficient process for the synthesis of 2d carbon nitrides and related materials, *Scientific Reports* 13 (1) (2023) 15423.
- [78] Y. Gong, M. Li, Y. Wang, Carbon nitride in energy conversion and storage: recent advances and future prospects, *ChemSusChem* 8 (6) (2015) 931–946.
- [79] J. Han, F. Wu, X. Chen, D. Hu, F. Yu, Y. Gao, B. Dai, W. Wang, et al., Nitrogen defects and porous self-supporting structure carbon nitride for visible light hydrogen evolution, *Journal of Materials Chemistry C* 11 (33) (2023) 11283–11294.
- [80] V. Patel, A. Baskar, S. Tiburcius, B. Morrison, B. Mod, P. S. Tanwar, P. Kumar, A. Karakoti, G. Singh, A. Vinu, Mesoporous carbon nitrides as emerging materials: Nanoarchitectonics and biosensing applications, *Advanced Sensor Research* 2 (9) (2023) 2300024.
- [81] C.-Y. Wang, K. Maeda, L.-L. Chang, K.-L. Tung, C. Hu, Synthesis and applications of carbon nitride (cnx) family with different carbon to nitrogen ratio, *Carbon* 188 (2022) 482–491.
- [82] K. Kumar, R. Kundu, Doping engineering in electrode material for boosting the performance of sodium ion batteries, *ACS Applied Materials*

- & Interfaces 16 (29) (2024) 37346–37362.
- [83] R. Shi, L. Liu, Y. Lu, C. Wang, Y. Li, L. Li, Z. Yan, J. Chen, Nitrogen-rich covalent organic frameworks with multiple carbonyls for high-performance sodium batteries, *Nature Communications* 11 (1) (2020) 178.
- [84] H.-T. Vuong, D.-V. Nguyen, L. P. Phuong, P. P. Minh, B. N. Ho, H. A. Nguyen, Nitrogen-rich graphitic carbon nitride (g-c₃n₅): Emerging low-bandgap materials for photocatalysis, *Carbon Neutralization* 2 (4) (2023) 425–457.
- [85] Z. Wang, Y. Jiang, Y. Hu, J. Li, X. Liu, K. Li, W. Cao, X. Xu, Y. Yang, K. Lin, New insights into co-pyrolysis among graphitic carbon nitride and organic compounds: carbonaceous gas fragments induced synthesis of ultrathin mesoporous nitrogen-doped carbon nanosheets for heterogeneous catalysis, *ACS Applied Materials & Interfaces* 12 (47) (2020) 52624–52634.
- [86] M. Skorupska, A. Ilnicka, J. P. Lukaszewicz, The effect of nitrogen species on the catalytic properties of n-doped graphene, *Scientific Reports* 11 (1) (2021) 23970.
- [87] M. Khosravifar, K. Dasgupta, V. K. R. Kondapalli, Y. Fang, R. Alexander, V. Shanov, Nitrogen-doped, vertically aligned structures of graphene and carbon nanofibers for energy storage applications, *ACS Applied Nano Materials* 7 (9) (2024) 10284–10292.
- [88] M. Liu, Y. Wen, L. Lu, Y. Chen, X. Tian, H. Jin, J. Liu, K. Dai, Nitrogen-doped graphene/graphitic carbon nitride with enhanced charge separation and two-electron-transferring reaction activity for boosting photocatalytic hydrogen peroxide production, *Sustainable Energy & Fuels* 5 (5) (2021) 1511–1520.
- [89] D. Mondal, A. Bandyopadhyay, A. Nandy, D. Jana, Intriguing topological signatures in newly predicted family of dumbbell c₃n_x (x = c, si, ge) and its quasi-1d derivatives, *Applied Materials Today* 40 (2024) 102360.
- [90] T. Li, C. He, W. Zhang, A novel porous c₄n₄ monolayer as a potential anchoring material for lithium-sulfur battery design, *Journal of materials chemistry A* 7 (8) (2019) 4134–4144.
- [91] W. Li, R. Tan, P. Zhou, L. Sun, A novel carbon–nitrogen dirac semimetal c₅n₄ monolayer, *Physica E: Low-dimensional Systems and Nanostructures* 143 (2022) 115350.
- [92] H. Chen, S. Zhang, W. Jiang, C. Zhang, H. Guo, Z. Liu, Z. Wang, F. Liu, X. Niu, Prediction of two-dimensional nodal-line semimetals in a carbon nitride covalent network, *Journal of Materials Chemistry A* 6 (24) (2018) 11252–11259.
- [93] Y. Li, S. Zhang, J. Yu, Q. Wang, Q. Sun, P. Jena, A new c = c embedded porphyrin sheet with superior oxygen reduction performance, *Nano Research* 8 (2015) 2901–2912.
- [94] R. Tan, X. Chen, L. Dai, Y. Ouyang, L. Cao, Z. Tang, M. Ma, X. Wei, G. Zhong, Strong mechanical anisotropy and an anisotropic dirac state in 2d c₅n₃, *Physical Chemistry Chemical Physics* 26 (15) (2024) 11782–11788.
- [95] J. Jin, G. Deokar, P. M. Costa, U. Schwingenschlögl, Monolayer c₅n: A promising building block for the anode of k-ion batteries, *Physical Review Applied* 17 (3) (2022) 034055.
- [96] Y. Kou, Y. Xu, Z. Guo, D. Jiang, Supercapacitive energy storage and electric power supply using an aza-fused π -conjugated microporous framework, *Angewandte Chemie* 123 (37) (2011) 8912–8916.
- [97] M. You, G. Guo, Y. Liao, S. Luo, C. He, C. Tang, J. Zhong, 2d novel c₅n₂ allotropes: High-performance anode materials for alkali metal ion battery, *Journal of Energy Storage* 84 (2024) 111004.
- [98] Z. Hajiahmadi, S. A. Ghasemi, T. D. Ku-hne, S. S. Naghavi, First-principles study of 2d haeckelite c₇n as a high-capacity anode for post-lithium-ion batteries, *ACS Applied Nano Materials* 6 (14) (2023) 12862–12870.
- [99] B. Mortazavi, M. Shahrokhi, A. V. Shapeev, T. Rabczuk, X. Zhuang, Prediction of c₇n₆ and c₉n₄: stable and strong porous carbon-nitride nanosheets with attractive electronic and optical properties, *Journal of Materials Chemistry C* 7 (35) (2019) 10908–10917.
- [100] S. Wolf, D. Awschalom, R. Buhrman, J. Daughton, v. S. von Molnár, M. Roukes, A. Y. Chtchelkanova, D. Treger, Spintronics: a spin-based electronics vision for the future, *science* 294 (5546) (2001) 1488–1495.
- [101] X. He, Y. Wang, N. Wu, A. N. Caruso, E. Vescovo, K. D. Belashchenko, P. A. Dowben, C. Binek, Robust isothermal electric control of exchange bias at room temperature, *Nature materials* 9 (7) (2010) 579–585.
- [102] J. S. Lee, X. Wang, H. Luo, S. Dai, Fluidic carbon precursors for formation of functional carbon under ambient pressure based on ionic liquids, *Advanced Materials* 22 (9) (2010) 1004–1007.

- [103] A. Du, S. Sanvito, S. C. Smith, First-principles prediction of metal-free magnetism and intrinsic half-metallicity in graphitic carbon nitride, *Physical review Letters* 108 (19) (2012) 197207.
- [104] K. Xu, X. Li, P. Chen, D. Zhou, C. Wu, Y. Guo, L. Zhang, J. Zhao, X. Wu, Y. Xie, Hydrogen dangling bonds induce ferromagnetism in two-dimensional metal-free graphitic- c_3n_4 nanosheets, *Chemical science* 6 (1) (2015) 283–287.
- [105] Z. Gao, H. Xiao, C. Zhang, C. He, J. Zhong, Ferromagnetism triggered by nitrogen defects in graphitic carbon nitride, *Journal of Physics D: Applied Physics* 53 (49) (2020) 495002.
- [106] Y. Yong, W. Zhang, Q. Hou, R. Gao, X. Yuan, S. Hu, Y. Kuang, Highly sensitive and selective gas sensors based on nanoporous cn monolayer for reusable detection of no, h₂s and nh₃: A first-principles study, *Applied Surface Science* 606 (2022) 154806.
- [107] H. Wang, Z. Chen, Z. Liu, Penta-cn₂ revisited: Superior stability, synthesis condition exploration, negative poisson's ratio and quasi-flat bands, *Applied Surface Science* 585 (2022) 152536.
- [108] Q. Guo, Q. Yang, C. Yi, L. Zhu, Y. Xie, Synthesis of carbon nitrides with graphite-like or onion-like lamellar structures via a solvent-free route at low temperatures, *Carbon* 43 (7) (2005) 1386–1391.
- [109] Z. Ma, X. Zhao, Q. Tang, Z. Zhou, Computational prediction of experimentally possible g-c₃n₃ monolayer as hydrogen purification membrane, *International journal of hydrogen energy* 39 (10) (2014) 5037–5042.
- [110] S. Singh, P. Anees, S. Chandra, T. K. Ghanty, Strain engineering of 2d-c₃n₅ monolayer and its application in overall water-splitting: a hybrid density functional study, *The Journal of Physical Chemistry C* 126 (19) (2022) 8436–8449.
- [111] T. Liu, G. Yang, W. Wang, C. Wang, M. Wang, X. Sun, P. Xu, J. Zhang, Preparation of c₃n₅ nanosheets with enhanced performance in photocatalytic methylene blue (mb) degradation and h₂-evolution from water splitting, *Environmental Research* 188 (2020) 109741.
- [112] P. Kumar, E. Vahidzadeh, U. K. Thakur, P. Kar, K. M. Alam, A. Goswami, N. Mahdi, K. Cui, G. M. Bernard, V. K. Michaelis, et al., C₃n₅: a low bandgap semiconductor containing an azo-linked carbon nitride framework for photocatalytic, photovoltaic and adsorbent applications, *Journal of the American Chemical Society* 141 (13) (2019) 5415–5436.
- [113] B. Mortazavi, F. Shojaei, M. Shahrokhi, M. Azizi, T. Rabczuk, A. V. Shapeev, X. Zhuang, Nanoporous c₃n₄, c₃n₅ and c₃n₆ nanosheets; novel strong semiconductors with low thermal conductivities and appealing optical/electronic properties, *Carbon* 167 (2020) 40–50.
- [114] I. Y. Kim, S. Kim, S. Premkumar, J.-H. Yang, S. Umapathy, A. Vinu, Thermodynamically stable mesoporous c₃n₇ and c₃n₆ with ordered structure and their excellent performance for oxygen reduction reaction, *Small* 16 (12) (2020) 1903572.
- [115] C. Yang, Z.-D. Yang, H. Dong, N. Sun, Y. Lu, F.-M. Zhang, G. Zhang, Theory-driven design and targeting synthesis of a highly-conjugated basal-plane 2d covalent organic framework for metal-free electrocatalytic oer, *ACS Energy Letters* 4 (9) (2019) 2251–2258.
- [116] C. Pu, D. Zhou, Y. Li, H. Liu, Z. Chen, Y. Wang, Y. Ma, Two-dimensional c₄n global minima: unique structural topologies and nanoelectronic properties, *The Journal of Physical Chemistry C* 121 (5) (2017) 2669–2674.
- [117] F. Huang, G. Liang, P. Zhou, Z. Ma, L. Sun, C₄n₄: A symmetry-protected semimetal, *Computational Materials Science* 224 (2023) 112165.
- [118] A. Bafekry, M. Shahrokhi, A. Shafique, H. Jappor, F. Shojaei, S. Feghhi, M. Ghergherehchi, D. Gogova, Two-dimensional carbon nitride c₆n nanosheet with egg-comb-like structure and electronic properties of a semimetal, *Nanotechnology* 32 (21) (2021) 215702.
- [119] C. He, M. Zhang, T. Li, W. Zhang, A novel c₆n₂ monolayer as a potential material for charge-controlled co₂ capture, *Journal of Materials Chemistry C* 8 (19) (2020) 6542–6551.
- [120] Y. Yuan, X. Song, B. Kang, J. Y. Lee, C₆n₃: A novel 2d carbon nitride with sp-n as support for efficient hydrogen production, *Journal of Colloid and Interface Science* 611 (2022) 472–479.
- [121] H. Li, H. Hu, C. Bai, C. Bao, F. Guo, Z. Feng, Y. Liu, The charge regulation of electronic structure and optical properties of graphitic carbon nitride under strain, *RSC advances* 9 (13) (2019) 7464–7468.
- [122] X. Zhao, Y. Zhao, H. Tan, H. Sun, X. Qin, W. Ho, M. Zhou, J. Lin, Y. Li, New carbon nitride close to c₆n₇ with superior visible light absorption for highly efficient photocatalysis, *Science Bulletin* 66 (17) (2021) 1764–1772.
- [123] A. Bafekry, M. Faraji, N. Hieu, A. B. Khatibani, M. M. Fadlallah, D. Gogova, M. Ghergherehchi, Tunable electronic properties of porous graphitic carbon nitride (c₆n₇) monolayer by atomic doping and embedding: A first-principle study, *Applied Surface Science* 583 (2022) 152270.

- [124] S. Hu, Y. Yong, Z. Zhao, R. Gao, Q. Zhou, Y. Kuang, C7n6 monolayer as high capacity and reversible hydrogen storage media: A dft study, *International Journal of Hydrogen Energy* 46 (42) (2021) 21994–22003.
- [125] H. Li, H. Hu, C. Bai, C. Bao, C. Liu, Q. Wang, F. Guo, Z. Feng, H. Yu, M. Chen, et al., Prediction of a stable organic metal-free porous material as a catalyst for water-splitting, *Catalysts* 10 (8) (2020) 836.
- [126] A. Kokabi, M. Fayazi, Noble metal single-atom catalyst supported by c8n8 monolayer as a promising reduction electrocatalyst for low-density environmental no, *Materials Today Communications* 37 (2023) 106831.
- [127] H. Xiang, B. Huang, Z. Li, S.-H. Wei, J. Yang, X. Gong, Ordered semiconducting nitrogen-graphene alloys, *Physical Review X* 2 (1) (2012) 011003.
- [128] X. Kan, Y. Ban, C. Wu, Q. Pan, H. Liu, J. Song, Z. Zuo, Z. Li, Y. Zhao, Interfacial synthesis of conjugated two-dimensional n-graphdiyne, *ACS applied materials & interfaces* 10 (1) (2018) 53–58.
- [129] K. Dabsamut, T. Maluangnont, P. Reunchan, S. Jungthawan, A. Boonchun, et al., Electric field-and strain-induced bandgap modulation in bilayer c2n, *Applied Physics Letters* 120 (20) (2022).
- [130] X. Niu, Y. Yi, X. Bai, J. Zhang, Z. Zhou, L. Chu, J. Yang, X. Li, Photocatalytic performance of few-layer graphitic c 3 n 4: enhanced by interlayer coupling, *Nanoscale* 11 (9) (2019) 4101–4107.
- [131] F. Dong, Z. Zhao, T. Xiong, Z. Ni, W. Zhang, Y. Sun, W.-K. Ho, In situ construction of g-c3n4/g-c3n4 metal-free heterojunction for enhanced visible-light photocatalysis, *ACS applied materials & interfaces* 5 (21) (2013) 11392–11401.
- [132] M. Mukherjee, R. Jana, A. Datta, Designing c 6 n 6/c 2 n van der waals heterostructures for photogenerated charge carrier separation, *Physical Chemistry Chemical Physics* 23 (6) (2021) 3925–3933.
- [133] C. He, Y. Liang, W. Zhang, Constructing a novel metal-free g-c3n4/g-cn vdw heterostructure with enhanced visible-light-driven photocatalytic activity for water splitting, *Applied Surface Science* 553 (2021) 149550.
- [134] G. Liao, C. Li, X. Li, B. Fang, Emerging polymeric carbon nitride z-scheme systems for photocatalysis, *Cell Reports Physical Science* 2 (3) (2021).
- [135] D. Zhao, Y. Wang, C.-L. Dong, Y.-C. Huang, J. Chen, F. Xue, S. Shen, L. Guo, Boron-doped nitrogen-deficient carbon nitride-based z-scheme heterostructures for photocatalytic overall water splitting, *Nature Energy* 6 (4) (2021) 388–397.
- [136] M. S. Akple, J. Low, S. Wageh, A. A. Al-Ghamdi, J. Yu, J. Zhang, Enhanced visible light photocatalytic h2-production of g-c3n4/ws2 composite heterostructures, *Applied Surface Science* 358 (2015) 196–203.
- [137] Y. Lin, Q. Wang, M. Ma, P. Li, V. Mahes Kumar, Z. Jiang, R. Zhang, Enhanced optical absorption and photocatalytic water splitting of g-c3n4/tio2 heterostructure through c&b codoping: A hybrid dft study, *International Journal of Hydrogen Energy* 46 (14) (2021) 9417–9432.
- [138] A. Ghosh, A. Pramanik, S. Pal, P. Sarkar, Emergence of z-scheme photocatalysis for total water splitting: An improvised route to high efficiency, *The Journal of Physical Chemistry Letters* 15 (26) (2024) 6841–6851.
- [139] Y. Wang, J. Lv, L. Zhu, Y. Ma, Crystal structure prediction via particle-swarm optimization, *Physical Review B* 82 (9) (2010) 094116.
- [140] S. Talatahari, M. Azizi, M. Tolouei, B. Talatahari, P. Sareh, Crystal structure algorithm (crystal): a metaheuristic optimization method, *IEEE Access* 9 (2021) 71244–71261.
- [141] C. W. Glass, A. R. Oganov, N. Hansen, Uspex—evolutionary crystal structure prediction, *Computer physics communications* 175 (11-12) (2006) 713–720.
- [142] A. R. Oganov, A. O. Lyakhov, M. Valle, How evolutionary crystal structure prediction works and why, *Accounts of chemical research* 44 (3) (2011) 227–237.
- [143] M. C. Burla, R. Caliendo, B. Carrozzini, G. L. Casciarano, C. Cuocci, C. Giacovazzo, M. Mallamo, A. Mazzone, G. Polidori, Crystal structure determination and refinement via sir2014, *Journal of Applied Crystallography* 48 (1) (2015) 306–309.
- [144] A. Altomare, N. Corriero, C. Cuocci, A. Falcicchio, A. Moliterni, R. Rizzi, Expo software for solving crystal structures by powder diffraction data: methods and application, *Crystal Research and Technology* 50 (9-10) (2015) 737–742.
- [145] R. Martoňák, A. Laio, M. Bernasconi, C. Ceriani, P. Raiteri, F. Zipoli, M. Parrinello, Simulation of structural phase transitions by metadynamics, *Zeitschrift für Kristallographie-Crystalline Materials* 220 (5-6) (2005) 489–498.

- [146] A. Cavalli, A. Spitaleri, G. Saladino, F. L. Gervasio, Investigating drug–target association and dissociation mechanisms using metadynamics-based algorithms, *Accounts of chemical research* 48 (2) (2015) 277–285.
- [147] R. Villarreal, P. Singh, R. Arroyave, Metric-driven search for structurally stable inorganic compounds, *Acta Materialia* 202 (2021) 437–447.
- [148] C.-N. Li, H.-P. Liang, X. Zhang, Z. Lin, S.-H. Wei, Graph deep learning accelerated efficient crystal structure search and feature extraction, *npj Computational Materials* 9 (1) (2023) 176.
- [149] G. G. Peterson, J. Brgoch, Materials discovery through machine learning formation energy, *Journal of Physics: Energy* 3 (2) (2021) 022002.
- [150] F. Faber, A. Lindmaa, O. A. Von Lilienfeld, R. Armiento, Crystal structure representations for machine learning models of formation energies, *International Journal of Quantum Chemistry* 115 (16) (2015) 1094–1101.
- [151] B. Mortazavi, I. S. Novikov, E. V. Podryabinkin, S. Roche, T. Rabczuk, A. V. Shapeev, X. Zhuang, Exploring phononic properties of two-dimensional materials using machine learning interatomic potentials, *Applied Materials Today* 20 (2020) 100685.
- [152] C. Cui, Y. Zhang, T. Ouyang, C. Tang, C. He, J. Li, M. Chen, J. Zhong, Machine learning interatomic potentials as efficient tools for obtaining reasonable phonon dispersions and accurate thermal conductivity: A case study of typical two-dimensional materials, *Applied Physics Letters* 123 (15) (2023).
- [153] A. Aizerman, Theoretical foundations of the potential function method in pattern recognition learning, *Automation and remote control* 25 (1964) 821–837.
- [154] B. Deng, P. Zhong, K. Jun, J. Riebesell, K. Han, C. J. Bartel, G. Ceder, Chgnet as a pretrained universal neural network potential for charge-informed atomistic modelling, *Nature Machine Intelligence* 5 (9) (2023) 1031–1041.
- [155] C. Chen, S. P. Ong, A universal graph deep learning interatomic potential for the periodic table, *Nature Computational Science* 2 (11) (2022) 718–728.
- [156] B. Mortazavi, Recent advances in machine learning-assisted multiscale design of energy materials, *Advanced Energy Materials* (2024) 2403876.
- [157] J. Behler, M. Parrinello, Generalized neural-network representation of high-dimensional potential-energy surfaces, *Physical review letters* 98 (14) (2007) 146401.
- [158] J. Wang, Y. Wang, H. Zhang, Z. Yang, Z. Liang, J. Shi, H.-T. Wang, D. Xing, J. Sun, E (n)-equivariant cartesian tensor message passing interatomic potential, *Nature Communications* 15 (1) (2024) 7607.
- [159] S. Choung, W. Park, J. Moon, J. W. Han, Rise of machine learning potentials in heterogeneous catalysis: Developments, applications, and prospects, *Chemical Engineering Journal* (2024) 152757.
- [160] I. S. Novikov, K. Gubaev, E. V. Podryabinkin, A. V. Shapeev, The mlip package: moment tensor potentials with mpi and active learning, *Machine Learning: Science and Technology* 2 (2) (2020) 025002.
- [161] B. Mortazavi, F. Shojaei, A. V. Shapeev, X. Zhuang, A combined first-principles and machine-learning investigation on the stability, electronic, optical, and mechanical properties of novel c6n7-based nanoporous carbon nitrides, *Carbon* 194 (2022) 230–239.
- [162] B. Mortazavi, A. Rajabpour, X. Zhuang, T. Rabczuk, A. V. Shapeev, Exploring thermal expansion of carbon-based nanosheets by machine-learning interatomic potentials, *Carbon* 186 (2022) 501–508.
- [163] B. Mortazavi, M. Shahrokhi, F. Shojaei, T. Rabczuk, X. Zhuang, A. V. Shapeev, A first-principles and machine-learning investigation on the electronic, photocatalytic, mechanical and heat conduction properties of nanoporous c 5 n monolayers, *Nanoscale* 14 (11) (2022) 4324–4333.
- [164] S. Arabha, A. Rajabpour, Thermo-mechanical properties of nitrogenated holey graphene (c2n): A comparison of machine-learning-based and classical interatomic potentials, *International Journal of Heat and Mass Transfer* 178 (2021) 121589.
- [165] S. Agrawal, B. Wang, Y. Wu, D. Casanova, O. V. Prezhdo, Photocatalytic activity of dual defect modified graphitic carbon nitride is robust to tautomerism: machine learning assisted ab initio quantum dynamics., *Nanoscale* (2024).
URL <https://api.semanticscholar.org/CorpusID:268860470>
- [166] W. Jeong, W. Sun, M. F. Calegari Andrade, L. F. Wan, T. M. Willey, M. H. Nielsen, T. A. Pham, Integrating machine learning potential and x-ray absorption spectroscopy for predicting the chemical speciation of disordered carbon nitrides, *Chemistry of Materials* 36 (9) (2024) 4144–4156.

- [167] K. Lee, D. Yoo, W. Jeong, S. Han, Simple-nn: An efficient package for training and executing neural-network interatomic potentials, *Computer Physics Communications* 242 (2019) 95–103.
- [168] X. Wan, W. Yu, H. Niu, X. Wang, Z. Zhang, Y. Guo, Revealing the oxygen reduction/evolution reaction activity origin of carbon-nitride-related single-atom catalysts: quantum chemistry in artificial intelligence, *Chemical Engineering Journal* 440 (2022) 135946.
- [169] M. Umer, S. Umer, M. Zafari, M. Ha, R. Anand, A. Hajibabaei, A. Abbas, G. Lee, K. S. Kim, Machine learning assisted high-throughput screening of transition metal single atom based superb hydrogen evolution electrocatalysts, *Journal of Materials Chemistry A* 10 (12) (2022) 6679–6689.
- [170] M. Jyothirmai, D. Roshini, B. M. Abraham, J. K. Singh, Accelerating the discovery of g-c3n4-supported single atom catalysts for hydrogen evolution reaction: a combined dft and machine learning strategy, *ACS Applied Energy Materials* 6 (10) (2023) 5598–5606.
- [171] M. Jyothirmai, R. Dantuluri, P. Sinha, B. M. Abraham, J. K. Singh, Machine-learning-driven high-throughput screening of transition-metal atom intercalated g-c3n4/mx2 (m= mo, w; x= s, se, te) heterostructures for the hydrogen evolution reaction, *ACS Applied Materials & Interfaces* (2024).
- [172] H. Niu, X. Wan, X. Wang, C. Shao, J. Robertson, Z. Zhang, Y. Guo, Single-atom rhodium on defective g-c3n4: a promising bifunctional oxygen electrocatalyst, *ACS Sustainable Chemistry & Engineering* 9 (9) (2021) 3590–3599.
- [173] P. A. Koyale, S. V. Mulik, J. L. Gunjekar, T. D. Dongale, V. B. Koli, N. B. Mullani, S. S. Sutar, Y. G. Kapdi, S. S. Soni, S. D. Delekar, Synergistic enhancement of water-splitting performance using mof-derived ceria-modified g-c3n4 nanocomposites: Synthesis, performance evaluation, and stability prediction with machine learning, *Langmuir* 0 (0) (0) null. doi:10.1021/acs.langmuir.4c01336.
- [174] X. Wan, W. Yu, A. Wang, X. Wang, J. Robertson, Z. Zhang, Y. Guo, High-throughput screening of gas sensor materials for decomposition products of eco-friendly insulation medium by machine learning, *ACS sensors* 8 (6) (2023) 2319–2330.
- [175] Q. Zhu, Y. Gu, X. Liang, X. Wang, J. Ma, A machine learning model to predict co2 reduction reactivity and products transferred from metal-zeolites, *ACS Catalysis* 12 (19) (2022) 12336–12348.
- [176] E. Moharramzadeh Goliaei, Photocatalytic efficiency for co2 reduction of co and cluster co2o2 supported on g-c3n4: A density functional theory and machine learning study, *Langmuir* 40 (15) (2024) 7871–7882. doi:10.1021/acs.langmuir.3c03550.
- [177] S. Xiang, P. Huang, J. Li, Y. Liu, N. Marcella, P. K. Routh, G. Li, A. I. Frenkel, Solving the structure of “single-atom” catalysts using machine learning–assisted xanes analysis, *Physical Chemistry Chemical Physics* 24 (8) (2022) 5116–5124.
- [178] F. Chen, Y. Yang, X. Chen, A first-principles and machine learning study on design of graphitic carbon nitride-based single-atom photocatalysts, *ACS Applied Nano Materials* (2024).
- [179] R. Ouyang, S. Curtarolo, E. Ahmetcik, M. Scheffler, L. M. Ghiringhelli, Sisso: A compressed-sensing method for identifying the best low-dimensional descriptor in an immensity of offered candidates, *Physical Review Materials* 2 (8) (2018) 083802.
- [180] L. Zhang, L. Chen, W. Zhao, Z. Hu, J. Chen, W. Zhang, J. Yang, Self-promoted ammonia selectivity for the electro-reduction of nitrogen on gt-c 3 n 4 supported single metal catalysts: the machine learning model and physical insights, *Inorganic Chemistry Frontiers* 10 (22) (2023) 6578–6587.
- [181] M. Mukherjee, S. Dutta, M. Ghosh, P. Basuchowdhuri, A. Datta, Performance of the nitrogen reduction reaction on metal bound gc 6 n 6: a combined approach of machine learning and dft, *Physical Chemistry Chemical Physics* 24 (28) (2022) 17050–17058.
- [182] J. Li, X. Liu, H. Wang, Y. Sun, F. Dong, Prediction and interpretation of photocatalytic no removal on g-c3n4-based catalysts using machine learning, *Chinese Chemical Letters* 35 (2) (2024) 108596.
- [183] M. Miodyńska, A. Mikolajczyk, P. Mazierski, T. Klimczuk, W. Lisowski, G. Trykowski, A. Zaleska-Medynska, Lead-free bismuth-based perovskites coupled with g-c3n4: A machine learning based novel approach for visible light induced degradation of pollutants, *Applied Surface Science* 588 (2022) 152921.
- [184] M. S. Dorraji, A. Amani-Ghadim, M. Rasoulifard, H. Daneshvar, B. S. Z. Aghdam, A. Tarighati, S. Hosseini, Photocatalytic activity of g-c3n4: An empirical kinetic model, optimization by neuro-genetic approach and identification of intermediates, *Chemical Engineering Research and Design* 127 (2017) 113–125.
- [185] A. Gordanshekan, S. Arabian, A. R. S. Nazar, M. Farhadian, S. Tangestaninejad, A comprehensive comparison of green bi2wo6/g-c3n4 and

- bi2wo6/tio2 s-scheme heterojunctions for photocatalytic adsorption/degradation of cefixime: Artificial neural network, degradation pathway, and toxicity estimation, *Chemical Engineering Journal* 451 (2023) 139067.
- [186] M. Sheydaei, B. Ayoubi-Feiz, G. Abbaszade-Fakhri, A visible-light active g-c3n4/ce-zno/ti nanocomposite for efficient photoelectrocatalytic pharmaceutical degradation: Modelling with artificial neural network, *Process Safety and Environmental Protection* 149 (2021) 776–785.
- [187] M. Qarajehdaghi, A. Mehrizad, P. Gharbani, G. H. Shahverdizadeh, Quaternary composite of cds/g-c3n4/rgo/cmc as a susceptible visible-light photocatalyst for effective abatement of ciprofloxacin: Optimization and modeling of the process by rsm and ann, *Process Safety and Environmental Protection* 169 (2023) 352–362.
- [188] C. Song, Y. Shi, M. Li, Y. He, X. Xiong, H. Deng, D. Xia, Prediction of g-c3n4-based photocatalysts in tetracycline degradation based on machine learning, *Chemosphere* (2024) 142632.
- [189] B. Gupta, A. K. Gupta, C. S. Tiwary, P. S. Ghosal, A multivariate modeling and experimental realization of photocatalytic system of engineered s-c3n4/zno hybrid for ciprofloxacin removal: influencing factors and degradation pathways, *Environmental research* 196 (2021) 110390.
- [190] J. Shan, X. Wu, C. Li, J. Hu, Z. Zhang, H. Liu, P. Xia, X. Huang, Photocatalytic degradation of tetracycline hydrochloride by a fe3o4/g-c3n4/rgo magnetic nanocomposite mechanism: modeling and optimization, *Environmental Science and Pollution Research* 30 (3) (2023) 8098–8109.
- [191] L. A. Taib, Rsm and ann methodologies in modeling the enhanced biodiesel production using novel protic ionic liquid anchored on g-c3n4@fe3o4 nanohybrid, *Chemosphere* (2024) 142399.
- [192] Z. Yu, D. Tang, Artificial neural network-assisted wearable flexible sweat patch for drug management in parkinson's patients based on vacancy-engineered processing of g-c3n4, *Analytical Chemistry* 94 (51) (2022) 18000–18008.
- [193] F. Li, H. Peng, N. Shen, C. Yang, L. Zhang, B. Li, J. He, Electrochemiluminescence in graphitic carbon nitride decorated with silver nanoparticles for dopamine determination using machine learning, *ACS Applied Materials & Interfaces* (2024).
- [194] X. Zhu, L. Gao, L. Tang, B. Peng, H. Huang, J. Wang, J. Yu, X. Ouyang, J. Tan, Ultrathin ptni nanozyme based self-powered photoelectrochemical aptasensor for ultrasensitive chloramphenicol detection, *Biosensors and Bioelectronics* 146 (2019) 111756.
- [195] P. Zhang, D. Sun, A. Cho, S. Weon, S. Lee, J. Lee, J. W. Han, D.-P. Kim, W. Choi, Modified carbon nitride nanozyme as bifunctional glucose oxidase-peroxidase for metal-free bioinspired cascade photocatalysis, *Nature communications* 10 (1) (2019) 940.
- [196] S. P. Das, R. Bhuyan, B. Baro, U. Das, R. Sharma, S. Bayan, Flexible triboelectric nanogenerators of au-g-c3n4/zno hierarchical nanostructures for machine learning enabled body movement detection, *Nanotechnology* 34 (44) (2023) 445501.
- [197] Y. Pathak, K. S. Juneja, G. Varma, M. Ehara, U. D. Priyakumar, Deep learning enabled inorganic material generator, *Physical Chemistry Chemical Physics* 22 (46) (2020) 26935–26943.
- [198] Y. Dan, Y. Zhao, X. Li, S. Li, M. Hu, J. Hu, Generative adversarial networks (gan) based efficient sampling of chemical composition space for inverse design of inorganic materials, *npj Computational Materials* 6 (1) (2020) 84.
- [199] Y. Song, E. M. D. Siriwardane, Y. Zhao, J. Hu, Computational discovery of new 2d materials using deep learning generative models, *ACS Applied Materials & Interfaces* 13 (45) (2021) 53303–53313.
- [200] C. J. Court, B. Yildirim, A. Jain, J. M. Cole, 3-d inorganic crystal structure generation and property prediction via representation learning, *Journal of Chemical Information and Modeling* 60 (10) (2020) 4518–4535.
- [201] Y. Zhao, M. Al-Fahdi, M. Hu, E. M. Siriwardane, Y. Song, A. Nasiri, J. Hu, High-throughput discovery of novel cubic crystal materials using deep generative neural networks, *Advanced Science* 8 (20) (2021) 2100566.
- [202] R. Gómez-Bombarelli, J. N. Wei, D. Duvenaud, J. M. Hernández-Lobato, B. Sánchez-Lengeling, D. Sheberla, J. Aguilera-Iparraguirre, T. D. Hirzel, R. P. Adams, A. Aspuru-Guzik, Automatic chemical design using a data-driven continuous representation of molecules, *ACS central science* 4 (2) (2018) 268–276.
- [203] J. Hu, M. Li, P. Gao, Matganip: Learning to discover the structure-property relationship in perovskites with generative adversarial networks, *arXiv preprint arXiv:1910.09003* (2019).
- [204] R. P. Joshi, J. Eickholt, L. Li, M. Fornari, V. Barone, J. E. Peralta, Machine learning the voltage of electrode materials in metal-ion batteries,

- ACS applied materials & interfaces 11 (20) (2019) 18494–18503.
- [205] A. Merchant, S. Batzner, S. S. Schoenholz, M. Aykol, G. Cheon, E. D. Cubuk, Scaling deep learning for materials discovery, *Nature* 624 (7990) (2023) 80–85.
- [206] H. Park, Z. Li, A. Walsh, Has generative artificial intelligence solved inverse materials design?, *Matter* 7 (7) (2024) 2355–2367.
- [207] D. Menon, R. Ranganathan, A generative approach to materials discovery, design, and optimization, *ACS omega* 7 (30) (2022) 25958–25973.
- [208] J. Arnold, F. Schäfer, A. Edelman, C. Bruder, Mapping out phase diagrams with generative classifiers, *Physical Review Letters* 132 (20) (2024) 207301.
- [209] O. Andreeva, W. Li, W. Ding, M. Kuijjer, J. Quackenbush, P. Chen, Catalysis clustering with gan by incorporating domain knowledge, in: *Proceedings of the 26th ACM SIGKDD international conference on knowledge discovery & data mining*, 2020, pp. 1344–1352.
- [210] A. Ishikawa, Heterogeneous catalyst design by generative adversarial network and first-principles based microkinetics, *Scientific Reports* 12 (1) (2022) 11657.
- [211] M. Z. Makoś, N. Verma, E. C. Larson, M. Freindorf, E. Kraka, Generative adversarial networks for transition state geometry prediction, *The Journal of Chemical Physics* 155 (2) (2021).
- [212] M. Manica, J. Born, J. Cadow, D. Christofidellis, A. Dave, D. Clarke, Y. G. N. Teukam, G. Giannone, S. C. Hoffman, M. Buchan, et al., Accelerating material design with the generative toolkit for scientific discovery, *npj Computational Materials* 9 (1) (2023) 69.

Name	Description
Amazon SageMaker	Fully managed service by AWS for building, training, and deploying ML models at scale, supporting various frameworks.
Azure ML	Cloud based service by Microsoft for building and deploying ML models, supporting automated ML and scalable computing resources.
Caffe	Deep learning framework with expressive architecture and model scalability, suitable for image recognition tasks.
caret	R package for data preprocessing, model training, and evaluation across various ML algorithms.
CatBoost	Gradient boosting library by Yandex with advanced handling of categorical features for ML tasks.
DataRobot	Automated ML platform for building and deploying ML models without extensive expertise.
Dask-ML	Scalable ML library compatible with scikit-learn APIs, designed for parallel and distributed computing with Dask.
H2O.ai	Open-source ML platform with scalable algorithms, AutoML, and support for multiple languages.
IBM Watson Studio	Integrated environment for data scientists and developers to build and deploy AI models using various open-source tools and IBM services.
KNIME	Open-source data analytics platform with visual programming interface for building data analysis workflows.
LightGBM	Gradient boosting framework by Microsoft for high-performance ML tasks with low memory usage.
MATLAB	Proprietary programming language and environment for numerical computing and ML.
ML.NET	Open-source ML framework by Microsoft for building and deploying ML models in .NET applications.
MLlib (Apache Spark)	Distributed ML library within Apache Spark for large-scale data processing and model training.
MXNet	Open-source deep learning framework for flexible and efficient model building and deployment.
Orange	Open-source tool for data visualization, analysis, and ML with a visual programming interface.
PyTorch	Open-source ML framework by Facebook, known for flexibility and ease of use in deep learning research.
RapidMiner	Integrated data science platform with visual workflow for data preparation, ML, and analytics.
scikit-learn	Python library for ML tasks such as classification, regression, and clustering.
Spark MLlib	Apache Spark's scalable ML library for distributed data processing and model training.
TensorFlow	Open-source ML framework by Google, supporting deep learning and scalable model deployment.
Theano	Python library for defining, optimizing, and evaluating mathematical expressions with support for deep learning.
Weka	Java based collection of ML algorithms and tools for data mining tasks.
XGBoost	Scalable and efficient gradient boosting library for ML tasks, known for high performance and accuracy.

Table 4: Platforms and Libraries for Machine Learning

Model	Pros	Cons
Linear Regression	Simple and interpretable Computationally efficient Well-established statistical metrics Good for linear relationships	Assumes linearity Sensitive to outliers Can't handle complex/non-linear patterns Assumes normality of residuals
Ridge Regression	Reduces overfitting with regularization Works well with multicollinearity Handles high-dimensional data effectively	Limited interpretability Cannot perform feature selection Regularization parameter needs tuning
Lasso Regression	Performs feature selection (shrinks coefficients to zero) Reduces overfitting Works well with sparse data	Can miss important variables Introduces bias Regularization parameter needs tuning
Elastic Net	Combines Ridge and Lasso strengths Good for high-dimensional and correlated data Performs both regularization and feature selection	More complex to tune (two hyperparameters) Less interpretable than Lasso alone
Polynomial Regression	Models non-linear relationships Flexible and adaptable	Risk of overfitting Higher complexity with degree of polynomial Can be hard to interpret
Support Vector Regression (SVR)	Works well in high-dimensional spaces Robust to overfitting Handles non-linear relationships via kernels	Computationally expensive Requires careful hyperparameter tuning Less interpretable
Decision Tree Regression	Easy to interpret Handles non-linear data No need for scaling or transformation Simple visualization of decisions	Prone to overfitting Sensitive to small data changes Instability with complex data
Random Forest Regression	Robust to overfitting Handles non-linearity Can handle missing data Good feature importance insights	Less interpretable Computationally intensive May overfit if not properly tuned
Gradient Boosting (XG-Boost, LightGBM)	High predictive power Handles complex non-linear relationships Flexible with loss functions Good feature importance	Computationally expensive Sensitive to hyperparameters Risk of overfitting if not tuned
K-Nearest Neighbors (KNN) Regression	Simple and intuitive No assumptions about data distribution Flexible and non-parametric	Slow at prediction time Sensitive to irrelevant features Needs feature scaling

Table 5: Pros and Cons of different regression models.

Model	Pros	Cons
Feedforward Neural Networks (FNN) / MLP	Simple architecture Universal approximation Versatile for regression	Prone to overfitting Slow training No temporal memory
Convolutional Neural Networks (CNNs)	Effective for images Parameter sharing Hierarchical feature learning	Requires large datasets Computationally expensive Fixed input size
Recurrent Neural Networks (RNNs)	Good for sequential data Handles temporal dependencies Flexible input length	Vanishing/exploding gradients Slow training Limited long-term memory
Long Short-Term Memory (LSTM)	Solves vanishing gradient problem Captures long-term dependencies Good for time series	Computationally expensive Slow training Not ideal for non-sequential tasks
Gated Recurrent Units (GRUs)	Simplified LSTM Effective for sequential data Faster training	Less memory retention Less interpretable Potentially lower performance than LSTM
Autoencoders	Dimensionality reduction Feature extraction Generative capabilities (e.g., VAEs)	Overfitting Poor reconstruction quality Limited interpretability
Generative Adversarial Networks (GANs)	Powerful for generative tasks Unsupervised learning Creative applications (e.g., art generation)	Training instability Requires fine-tuning Hard to evaluate generated data
Transformer Networks	State-of-the-art performance Parallelizable Effective for sequential data	Data-hungry Computationally expensive Memory intensive
Capsule Networks (CapsNets)	Better generalization Resistant to spatial transformations Dynamic routing of information	Unstable training Limited practical benchmarks Slow convergence
Self-Organizing Maps (SOMs)	Unsupervised learning Topological preservation Interpretability	Slow training Limited for non-linear tasks Hard to scale

Table 6: Pros and Cons of different ANN architectures.

Platform/Framework	Description and Applications
OpenAI GPT	Language model for text generation and understanding. Used in chatbots, content generation, translation.
DeepMind AlphaFold	AI system predicting protein structures based on amino acid sequences. Applications in bioinformatics and drug discovery.
NVIDIA GANs (e.g., StyleGAN)	Frameworks for generating high-quality images and manipulating visual content. Used in art generation, image synthesis, video creation.
TensorFlow	Google's open-source framework for building and deploying ML models, including generative models like VAEs and GANs.
PyTorch	Facebook's open-source framework known for its dynamic approach to neural networks. Used in research and production of generative models.
Hugging Face Transformers	Library for working with transformers, including pre-trained models like BERT and GPT. Applications in text generation, sentiment analysis, and translation.
Google Cloud AI Platform	Suite of AI services offering pre-trained models and tools for custom model development and deployment.
AWS AI Services	Amazon's AI services providing pre-trained models and infrastructure for building custom AI solutions using TensorFlow, PyTorch, etc.
Microsoft Azure AI	Cognitive services and ML tools for developing and deploying generative models, supporting custom AI solutions.

Table 7: Online Platforms and Frameworks for Generative AI

Name	Short Description	Website
AFLOW & AFlowLib	Automatic Flow for Materials Discovery, providing data and software.	aflow.org aflowlib.org
AiiDA	Flexible and scalable informatics infrastructure to manage, preserve, and disseminate the computational data.	aiida.net
Atomate	A high-level Python framework for automating computational workflows.	atomate.org
C2DB	The Computational Crystallography Database of 2D materials.	cmr.fysik.dtu.dk/c2db/c2db.html
ChemAI	An AI platform focusing chemical and materials discovery.	acnetwork.nl/chemai
Citrine Informatics	Provides AI driven materials data and tools for materials discovery and optimization.	citrine.io
DeepChem	An open-source deep-learning library applicable to chemistry and materials science.	deepchem.io
Exabyte.io	A cloud based platform for computational materials science and chemistry simulations.	exabyte.io
Granta MI	Materials information management software for managing and analysing materials data.	grantami.com
HTEM DB	High Throughput Experimental Materials Database.	htem.nrel.gov
JARVIS	Joint Automated Repository for Various Integrated Simulations for materials data and tools.	jarvis.nist.gov
Khazana	A data repository for ML in chemistry and materials science.	khazana.gatech.edu
Magpie	A ML package for materials data and prediction.	bitbucket.org/wolverton/magpie
MAST-ML	An open-source tool for ML in materials science.	mastml.org
Materials Cloud	Repository of open-access research data in computational materials science.	materialscloud.org
Materials Data Facility	A repository and data resource that enables the publication, discovery, and access to materials data.	materialsdatafacility.org
Materials Project	Provides open web based access to computed information on known and predicted materials.	materialsproject.org
MatWeb	An online database for materials properties and ML models.	matweb.com
Material Bank	A repository of materials data for use in ML and materials research.	materialbank.org
Matbench	A benchmark suite for evaluating ML models in materials science.	matbench.materialsproject.org
MatDL	Materials Data Lab, a platform for materials data management and analysis.	matdl.org
Matminer	A library that contains tools to apply data mining and ML techniques to materials science.	hackingmaterials.lbl.gov/matminer
MatSci ML	A platform focused on ML applications in materials science.	github.com/IntelLabs/matsciml
MPContribs	A web platform to upload, share, and discuss contributions to the Materials Project database.	mpcontribs.org
MPDS	Materials Platform for Data Science, a platform for materials data and tools.	mpds.io
MDAnalysis	A Python library to analyse molecular dynamics simulations, providing data and tools for materials science.	mdanalysis.org
NREL Materials Database	A repository of data on materials for energy applications.	materials.nrel.gov
NOMAD	The Novel Materials Discovery (NOMAD) repository contains a vast amount of materials data and offers tools for their analysis.	nomad-coe.eu
OMDB	Organic Materials Database provides access to electronic structure properties of previously synthesized compounds.	omdb.mathub.io/
OQMD	The Open Quantum Materials Database is a database of DFT-calculated thermodynamic and structural properties of materials.	oqmd.org
Open Materials Database	A database for open access to materials data for research and development.	openmaterialsdb.se
QM9 Database	A database of small organic molecules for quantum ML models.	quantum-machine.org/datasets/
ThermoML	An IUPAC standard XML based approach for storage and exchange of experimental and critically evaluated thermophysical and thermochemical property data.	trc.nist.gov/ThermoML
Thermtest	A database for thermophysical properties of materials.	thermtest.com/thermal-resources/materials-database

Table 8: Different repositories targeted for Machine Learning in Material Science

Name	Short Description	Website
CatLearn	An open-source Python library for ML in catalysis.	catlearn.org
Catalysis-Hub	A platform providing access to data and tools for research in catalysis.	catalysis-hub.org
Catalysis Knowledge	Provides access to a comprehensive database of catalytic materials and related data.	catalysisknowledge.com
Catalyst Design	A platform for designing and optimizing catalysts using ML.	catalystdesign.org
CMR	Catalyst Materials Repository, a database for catalyst materials and their properties.	catalystmaterials.org
Open Catalyst Project	An open-source project for developing ML models for catalysis.	opencatalystproject.org
Reaction Mechanism Generator (RMG)	An open-source software for automatic generation of chemical reaction mechanisms.	rmg.mit.edu
XDL	An open-source language for describing experiments in catalysis and other fields.	xdl.org
CatApp	Catalysis Applications Database for accessing and sharing catalytic data.	catapp.org
ChemTS	An AI tool for automated molecular design for catalysis	chemts.kazusa.or.jp
ChemCatBio	Consortium focused on catalysis for biofuels and bio based chemicals.	chemcatbio.org
Catalysis Data Science	A platform for data science approaches in catalysis research.	catalysisdatascience.org
CatDATA	A database for catalyst characterization and performance data	catdata.org
CatKB	The Catalysis Knowledge Base, a comprehensive resource for catalytic data and information.	catkb.org
Catalyst Informatics	A platform for integrating informatics tools in catalyst design and optimization.	catalystinformatics.org
ChemHTPS	High-throughput computational screening platform for catalysis.	chemhttps.org

Table 9: Projects on Machine Learning in Catalysis